Pergamon

Geochimica et Cosmochimica Acta, Vol. 67, No. 23, pp. 4621–4638, 2003

0016-7037/03 $30.00 + .00

doi:10.1016/S0016-7037(03)00383-1

Factors controlling compositions of cosmic spinels: Application to atmospheric entry conditions of meteoritic materials

A. TOPPANI[1,2,*] and G. LIBOUREL[1,3]

[1]Centre de Recherche Pétrographiques et Géochimiques, CNRS-UPR2300, BP20, 54501 Vandoeuvre-les-Nancy, France
[2]MNHN, Laboratoire d'Etude de la Matière Extraterrestre, UMS CNRS 2679, 61 rue Buffon, 75005 Paris, France
[3]Ecole Nationale Supérieure de Géologie, INPL, BP40, 54501 Vandoeuvre-les-Nancy, France

(*Received February* 11, 2003; *accepted in revised form May* 19, 2003)

Abstract—During their deceleration through the Earth's atmosphere, meteoritic materials, i.e., interplanetary dust particles, micrometeorites and meteorites, experience thermal shocks which may alter their pristine mineralogy, texture or chemical characteristics. Among these changes, one of the most ubiquitous is the formation of spinels resulting from partial melting and subsequent crystallization of the meteoritic material. These "cosmic spinels" differ from terrestrial spinels by their high Ni and Fe^{3+} contents and show large variations in composition. In order to better understand the factors controlling their chemistry, pulse-heating experiments simulating atmospheric entry of extraterrestrial objects were carried out using Orgueil samples as proxies of meteoritic material. Covering a large range of experimental conditions (temperature 500°C $<$ T $<$1500°C, duration: 5 s $<$ t $<$ 120 s, and oxygen fugacity: $-0.68 < \log fO_2 < -8$), this work shows (1) that the whole range of composition of cosmic spinels analyzed so far at the micrometer scale in fine-grained and scoriaceous micrometeorites, in cosmic spherules or in the fusion crust of several stony meteorites can be reproduced, and (2) that these compositional changes can be expressed as a function of temperature, time and oxygen fugacity.

We also show that, due to their fast crystallization kinetics, cosmic spinels can record through their composition, i.e., Al_2O_3 contents and FeO/Fe_2O_3 ratio, the diverse conditions of the atmosphere crossed by the extraterrestrial object during its fall towards the Earth's surface. Chemistry of cosmic spinels is thus a powerful tool for constraining the entry conditions in the Earth's atmosphere of any extraterrestrial object, including altitude of deceleration, entry angle and incident velocity. These in turn, may provide valuable information on the origin of the extraterrestrial material.

1. INTRODUCTION

Depending on their mass, size, speed and entry angle, extraterrestrial objects (IDPs, micrometeorites and meteorites) decelerating in the Earth's atmosphere suffer different degrees of heating (Whipple, 1951; Fraundorf, 1980; Flynn, 1989; Love and Brownlee, 1991; Hills and Goda, 1993), which lead to various textural, mineralogical and chemical changes. Among these changes, one of the most ubiquitous is the formation of spinels, referred to by Robin et al. (1992) as cosmic spinels. Excluding spinels from the KT boundary sediments (see below), these spinels are generally observed in IDPs (Germani et al., 1990; Keller et al., 1992, 1993, 1996), in micrometeorites (MMs) constituting the "magnetite shell" (Maurette et al., 1991; Kurat et al., 1994; Genge et al., 1997; Engrand and Maurette, 1998), in cosmic spherules (e.g., Blanchard et al., 1980; Brownlee et al., 1997) and in fusion crusts of some stony meteorites (Ramdohr, 1967; Fruland, 1974; Genge and Grady, 1999). Based on previous pulse-heating experiments, Toppani et al. (2001) have shown that spinels in MMs and cosmic spherules (Jessberger et al., 1992; Kurat et al., 1994; Maurette, 1998) are formed by crystallization from a melt produced by partial melting of the meteoritic material during their entry in the Earth's atmosphere, as is also true for the spinels of fusion crusts (Genge and Grady, 1999). Furthermore, depending on temperature, run time and oxygen fugacity of the heating-pulse, these experiments also demonstrated that it is possible to reproduce (i) the different types of MMs described in the literature (Genge et al., 1997), including fine-grained particles encapsulated by very thin spinel rims, scoriaceous particles surrounded by well-developed continuous spinel rims and more extensively molten particles (cosmic spherules) showing large spinels and anhydrous silicate crystals, as well as (ii) the texture of the fusion crusts of some stony meteorites (Genge and Grady, 1999).

These cosmic spinels differ from terrestrial ones (Robin et al., 1992; Barnes and Roeder, 2001) principally by their higher nickel and ferric iron contents. Furthermore, they show a large range of compositions which can be attributed to differences in bulk composition and/or in entry conditions in the Earth's atmosphere. However, despite this variability, few studies (Robin et al., 1992; Gayraud et al., 1996) were devoted to understanding the peculiar compositions of these spinels. Indeed, whereas numerous experiments focused on understanding the crystallization of terrestrial spinels under equilibrium conditions (e.g., Hill and Roeder, 1974; Fisk and Bence, 1980; Maurel and Maurel, 1982a,b, 1983, 1984; Barnes and Roeder, 2001), only a few were carried out on extraterrestrial materials (Gayraud et al., 1996) at timescales relevant to the formation of cosmic spinels, i.e., a few seconds to a few tens of seconds (e.g., Hallyday et al., 1989; Love and Brownlee, 1991; Rietmeijer, 2000).

In this paper, we show that, using a set of pulse-heating

* Author to whom correspondence should be addressed (toppani@crpg.cnrs-nancy.fr).

Table 1. Temperature, time and oxygen fugacity conditions of pulse-heating experiments of Orgueil fragments

Run	Temperature (°C)	Gas	$Log_{10}fO_2$	Duration (s)
50/1/20	500	Air	−0.68	20
80/1/20	800	Air	−0.68	20
100/1/20	1000	Air	−0.68	20
100/2/20	1000	96.5% CO_2 + 3.5% N_2	−4.92	20
120/1/5, 10, 20*, 40*, 120*	1200	Air	−0.68	5, 10, 20, 40, 120
120/2/5, 10*, 20*, 120*	1200	CO_2	−3.86	5, 10, 20, 120
120/3/10*, 20*, 40*, 120*	1200	99.6% CO_2 + 0.4% CO	−6.18	10, 20, 40, 120
135/1 2, 5*, 10*, 20*, 40*, 120*	1350	Air	−0.68	2, 5, 10, 20, 40, 120
135/2 2, 5*, 10*, 20*, 40*, 120*, 240*	1350	96.5% CO_2 + 3.5% N_2	−3.26	2, 5, 10, 20, 40, 120, 240
135/3 5*, 40*, 120*	1350	77.8% CO_2 + 20.2% N_2 + 2% CO	−5.96	5, 40, 120
135/4 20*, 40*, 120*	1350	6.8% CO_2 + 91.2% N_2 + 2% CO	−8	20, 40, 120
142/1/5*, 10*, 20*, 40*, 120*	1425	Air	−0.68	5, 10, 20, 40, 120
142/2/5*, 20*, 40*, 120*	1425	41.4% CO_2 + 58.6% N_2	−3.27	5, 20, 40, 120
142/3/40*, 120*	1425	27% CO_2 + 71% N_2 + 2% CO	−6.08	40, 120
150/1/5*, 120*	1500	Air	−0.68	5, 120
150/2/10*, 120*	1500	17.3% CO_2 + 82.7% N_2	−3.27	10, 120
150/3/5*, 120*	1500	13.5% CO_2 + 84.5% N_2 + 2% CO	−5.96	5, 120

Abbreviations: run 142/1/5 designates a run carried out at 1425°C (142) under an oxygen fugacity of −0.68 log units (atmosphere of type 1) during 5 s (5). Atmospheres of type 1, 2, 3, 4 correspond respectively to oxygen fugacity of ~−0.68, ~−3.5, ~−6, ~−8 log units.

* Occurrence of crystallized spinels in the pulse-heated samples.

experiments, it is possible to reproduce the whole compositional range of these "cosmic spinels" and to model their variability in composition as a function of temperature, heating time and oxygen fugacity. As "cosmic spinels" form during the deceleration of extraterrestrial objets in the Earth's atmosphere, this work also shows that their compositions can be used to determine (1) the types of extraterrestrial objects from which they were derived, (2) the entry conditions of these objects, and eventually, (3) where these objects originated.

2. EXPERIMENTAL METHOD

Pulse-heating experiments (Toppani et al., 2001, and this study) were carried out over temperatures from 500°C to 1500°C for run times between 5 and 120 s. These experiments were designed (i) to simulate the entry conditions of micrometeorites (Love and Brownlee, 1991) and meteorites (Rietmeijer, 2000), and (ii) to evaluate the effect of kinetics on spinel composition. Because MMs and meteorites decelerate at different altitudes (Love and Brownlee, 1991; Rietmeijer and Nuth, 2000), experiments were performed over oxygen fugacities ranging from log $fO_2 = -0.68$ to -8 to simulate the terrestrial atmosphere from the ground to the thermosphere, i.e., to altitudes circa 120 km. For all experiments, the total pressure was fixed at 1 bar (see Toppani et al., 2001). Experimental conditions are listed in Table 1.

2.1. Starting Materials

Fragments 200–400 μm in size of Orgueil (CI chondrite) were used as starting materials. Orgueil consists mainly of an homogeneous hydrated matrix rich in phyllosilicates (e.g., Böstrom and Fredriksson, 1966; Tomeoka and Buseck, 1988). Even if CM chondrite material may resemble MMs more closely (e.g., Kurat et al., 1994; Engrand and Maurette, 1998), the choice of Orgueil, offers the possibility (i) to carry out this study using a fairly homogeneous material, (ii) to mimic the MMs since unmelted MMs are dominated by phyllosilicates and (iii) to represent the mean composition of the matrix of numerous meteorites.

2.2. Experimental Techniques

As described in Toppani et al. (2001), experiments were performed at atmospheric pressure in a 1700°C GERO HTVR 70-250 closed vertical furnace (CRPG-CNRS, Nancy). Oxygen fugacity (fO_2) in each experiment was controlled by either CO_2-N_2 or CO_2-CO-N_2 gas mixtures, fed to the furnace at flow rates of 300 $cm^3.min^{-1}$. The oxygen fugacity, established in the furnace before each experiment was checked using a fixed yttrium-stabilized zirconia oxygen sensor.

Pairs of Orgueil fragments having a size of two hundred to four hundred micrometers were inserted into tiny platinum wire spiral holders, loaded into the hotspot of the furnace and quenched in air after pulse-heating experiments.

2.3. Analytical Methods

Experimental charges were embedded in epoxy resin and polished. The analyses of spinels were performed using a fully automated Cameca SX50 electron microprobe at the Université Henri Poincaré, Nancy (France). An accelerating potential of 15 kV, a beam current of 10 nA and a counting time of 30 s were employed. Analyses were obtained using a focused beam. Data were reduced by the ZAF method.

One of the main difficulty encountered during probe session analyses was the smallness of spinel crystals in many of our experimental runs (<10 μm), which had led to various amounts of contamination. Because analyses of small spinel crystals could be biased by significant contributions from the surrounding silicate mesostasis (crystalline or glassy), spinel analyses with $SiO_2 > 1$ wt% were systematically discarded. In some charges, all spinel analyses were contaminated and are only given here for indication (Table 2). No corrections of spinel analyses were carried out using compositions of the adjacent phases.

The use of platinum holders in experimental petrology is very often a possible source of sample iron loss. However, Toppani et al. (2001) have shown that for our experiments this problem is minor due to the spatial arrangement of the Orgueil chips in the Pt holders, to the short duration and the relatively oxidizing conditions of the experiments and to precautions taken during the electron microprobe analyses.

2.4. Data Reduction

The spinel structure is given as AB_2O_4, where A is the tetrahedral site and B the octahedral site. To neutralize the 8 negative charges of the oxygen, divalent (Mg^{2+}, Mn^{2+}, Fe^{2+}, Ni^{2+}), trivalent (Al^{3+}, Cr^{3+}, Fe^{3+}) or tetravalent (Ti^{4+} and Si^{4+}) cations fill the sites A or B. According to the distribution of these cations in the two sites, normal, inverse or intermediate spinels can be distinguished. Here, the FeO/Fe_2O_3 ratios of spinels (Table 2) were calculated assuming that spinel is stoichiometric, i.e., the sum of divalent and tetravalent cations (Mg^{2+}, Mn^{2+}, Fe^{2+}, Ni^{2+}, Ti^{4+} and Si^{4+}) is equal to half the sum of trivalent cations (Al^{3+}, Cr^{3+}, Fe^{3+}).

As spinel belongs to a complex solid-solution, its composition has also been recast in terms of the following end-members: magnetite

Table 2. Compositions of spinels (wt%) (electron microprobe analyses) of heated Orgueil fragments (see experimental conditions in Table 1)

Run	n	SiO_2	TiO_2	Al_2O_3	Cr_2O_3	Fe_2O_3	FeO	MnO	MgO	NiO	Total	FeO/Fe_2O_3
50/1/20	7	0.2 (0.15)	0.0 (0.06)	0.0 (0.02)	0.1 (0.02)	66.6 (0.49)	30.5 (0.46)	0.0 (0.03)	0.0 (0.03)	0.1 (0.09)	97.6 (0.65)	0.46 (0.01)
80/1/20	5	0.1 (0.09)	0.0 (0.03)	0.0 (0.00)	0.1 (0.05)	66.3 (1.06)	30.0 (0.58)	0.1 (0.07)	0.0 (0.02)	0.1 (0.09)	96.7 (1.60)	0.45 (0.00)
120/1/5	3	0.2 (0.12)	0.0 (0.03)	0.0 (0.02)	0.1 (0.04)	65.4 (1.82)	29.2 (0.60)	0.1 (0.11)	0.3 (0.30)	0.1 (0.09)	95.4 (2.49)	0.45 (0.01)
120/1/10	3	0.2 (0.23)	0.0 (0.01)	0.0 (0.04)	0.0 (0.04)	64.9 (0.49)	28.5 (0.97)	0.0 (0.02)	0.6 (0.88)	0.1 (0.16)	94.4 (0.58)	0.44 (0.01)
120/1/20	4	0.3 (0.09)	0.0 (0.03)	0.3 (0.12)	0.1 (0.03)	70.4 (1.63)	10.6 (3.29)	0.5 (0.30)	11.3 (1.49)	1.6 (0.83)	95.1 (1.88)	0.15 (0.05)
120/1/40	5	0.4 (0.14)	0.0 (0.03)	0.5 (0.31)	0.1 (0.06)	70.9 (0.84)	9.5 (2.97)	0.4 (0.26)	12.4 (1.46)	1.3 (0.55)	95.5 (1.35)	0.13 (0.04)
120/1/120	5	0.4 (0.31)	0.1 (0.03)	0.6 (0.12)	0.0 (0.03)	73.0 (1.17)	5.7 (1.53)	0.6 (0.11)	14.3 (1.25)	2.7 (1.86)	97.4 (0.91)	0.08 (0.02)
120/2/5	2	0.0 (0.00)	0.0 (0.05)	0.0 (0.01)	0.1 (0.03)	65.0 (1.48)	28.9 (0.98)	0.0 (0.00)	0.2 (0.06)	0.1 (0.13)	94.3 (2.28)	0.45 (0.00)
120/2/10	6	0.3 (0.27)	0.0 (0.00)	0.1 (0.07)	0.1 (0.02)	67.2 (3.12)	19.2 (1.85)	0.1 (0.04)	6.4 (1.59)	0.5 (0.24)	93.8 (3.77)	0.29 (0.04)
120/2/20	2	0.7 (0.14)	0.0 (0.00)	0.4 (0.15)	0.0 (0.00)	68.7 (0.37)	15.9 (0.71)	0.4 (0.08)	8.5 (0.71)	1.5 (0.23)	96.1 (0.21)	0.23 (0.01)
120/2/120	6	0.4 (0.35)	0.1 (0.05)	1.0 (0.35)	0.1 (0.05)	67.3 (1.77)	19.1 (3.43)	0.3 (0.08)	5.7 (2.04)	2.8 (0.68)	96.7 (1.05)	0.28 (0.06)
120/3/10	6	0.1 (0.08)	0.0 (0.04)	0.0 (0.04)	0.0 (0.04)	68.2 (1.15)	26.8 (1.39)	0.1 (0.08)	2.1 (0.98)	0.4 (0.16)	97.9 (1.19)	0.39 (0.03)
120/3/20	8	0.1 (0.08)	0.0 (0.01)	0.1 (0.05)	0.0 (0.04)	68.8 (1.18)	23.9 (2.50)	0.1 (0.08)	3.4 (1.19)	1.1 (1.10)	97.6 (1.10)	0.36 (0.04)
120/3/40	11	0.7 (0.36)	0.0 (0.05)	1.2 (0.98)	0.1 (0.04)	63.4 (2.02)	23.6 (1.71)	0.1 (0.12)	3.1 (1.33)	2.0 (0.93)	94.3 (1.59)	0.37 (0.03)
120/3/120	9	0.5 (0.32)	0.1 (0.14)	1.3 (0.56)	0.1 (0.06)	64.7 (1.88)	20.5 (1.43)	0.2 (0.08)	4.8 (0.89)	2.3 (0.63)	94.4 (1.35)	0.32 (0.02)
135/1/2	6	0.0 (0.03)	0.0 (0.03)	0.0 (0.02)	0.0 (0.05)	68.4 (0.66)	30.8 (0.29)	0.0 (0.02)	0.0 (0.05)	0.1 (0.06)	99.4 (0.95)	0.45 (0.00)
135/1/5	10	0.3 (0.22)	0.0 (0.03)	0.2 (0.12)	0.0 (0.03)	70.2 (1.64)	17.0 (4.26)	0.2 (0.11)	8.2 (2.79)	0.6 (0.31)	96.7 (0.65)	0.24 (0.07)
135/1/10	14	0.3 (0.31)	0.0 (0.03)	0.3 (0.19)	0.1 (0.04)	71.1 (1.55)	14.9 (4.46)	0.5 (0.21)	9.2 (2.88)	1.2 (0.84)	97.7 (1.03)	0.21 (0.07)
135/1/20	17	0.3 (0.29)	0.0 (0.04)	1.0 (0.36)	0.1 (0.06)	71.4 (1.12)	12.3 (2.11)	0.3 (0.07)	11.1 (1.30)	1.4 (0.38)	97.9 (0.86)	0.17 (0.03)
135/1/40	12	0.4 (0.29)	0.0 (0.05)	1.2 (0.18)	0.2 (0.29)	71.7 (1.39)	10.5 (0.89)	0.3 (0.14)	11.4 (0.71)	3.1 (0.91)	98.8 (0.97)	0.15 (0.01)
135/1/120	10	0.3 (0.28)	0.0 (0.03)	1.6 (0.10)	0.4 (0.25)	71.1 (1.08)	9.9 (0.75)	0.3 (0.11)	11.3 (0.29)	3.8 (0.49)	98.7 (0.80)	0.14 (0.01)
135/2/2	7	0.2 (0.18)	0.0 (0.04)	0.0 (0.01)	0.1 (0.04)	67.4 (1.10)	30.6 (0.60)	0.0 (0.05)	0.1 (0.07)	0.1 (0.07)	98.4 (1.58)	0.45 (0.01)
135/2/5	11	0.5 (0.26)	0.1 (0.06)	0.6 (0.22)	0.0 (0.04)	65.2 (1.39)	21.5 (1.98)	0.2 (0.10)	4.4 (1.24)	1.4 (0.93)	93.9 (1.73)	0.33 (0.03)
135/2/10	13	0.7 (0.40)	0.1 (0.11)	1.2 (0.42)	0.1 (0.06)	65.9 (1.30)	20.2 (2.31)	0.2 (0.16)	5.8 (1.44)	1.8 (0.76)	96.0 (0.90)	0.31 (0.03)
135/2/20	27	0.4 (0.28)	0.1 (0.13)	1.4 (0.57)	0.1 (0.12)	68.4 (1.83)	17.2 (2.07)	0.3 (0.09)	7.5 (1.14)	2.2 (0.77)	97.5 (1.65)	0.25 (0.03)
135/2/40	8	0.7 (0.19)	0.1 (0.05)	2.2 (0.06)	0.4 (0.22)	64.4 (0.67)	16.8 (0.86)	0.2 (0.06)	7.1 (0.61)	2.8 (0.21)	94.7 (0.77)	0.26 (0.01)
135/2/120	11	0.3 (0.12)	0.1 (0.06)	1.9 (0.24)	0.6 (0.85)	67.4 (1.38)	16.7 (0.59)	0.2 (0.13)	7.1 (0.28)	3.3 (0.51)	97.7 (1.41)	0.25 (0.01)
135/2/240	9	0.1 (0.09)	0.1 (0.05)	1.9 (0.26)	0.4 (0.28)	69.3 (1.15)	15.9 (1.05)	0.5 (0.21)	7.3 (0.67)	4.0 (0.47)	99.6 (1.06)	0.23 (0.02)
135/3/40	6	5.6 (1.90)	0.1 (0.06)	2.5 (0.57)	0.7 (0.80)	55.7 (5.44)	19.7 (1.88)	0.4 (0.04)	11.0 (1.09)	1.2 (0.46)	96.9 (1.90)	0.36 (0.06)
135/3/120	13	0.6 (0.26)	0.4 (0.15)	8.2 (2.92)	15.5 (6.47)	41.8 (5.57)	21.9 (1.15)	0.2 (0.12)	5.6 (0.90)	2.0 (0.44)	96.1 (0.62)	0.52 (0.09)
135/4/20	6	3.3 (1.25)	0.2 (0.05)	2.6 (0.53)	0.2 (0.16)	60.0 (3.90)	19.8 (2.42)	0.5 (0.14)	9.1 (1.83)	0.7 (0.58)	96.4 (1.96)	0.33 (0.06)
135/4/40	4	1.7 (0.89)	0.3 (0.19)	3.7 (2.38)	1.1 (0.97))	57.4 (2.14)	24.4 (2.55)	0.2 (0.17)	4.4 (3.30)	1.2 (0.59)	94.4 (6.12)	0.42 (0.04)
135/4/120	4	5.3 (1.21)	0.2 (0.08)	3.4 (0.98)	0.6 (0.34)	54.1 (4.96)	23.5 (6.25)	0.5 (0.14)	8.7 (2.70)	0.7 (0.29)	96.9 (1.13)	0.44 (0.16)
142/1/5	6	0.4 (0.22)	0.0 (0.02)	0.5 (0.15)	0.0 (0.05)	71.6 (0.88)	11.2 (2.04)	0.4 (0.13)	11.5 (1.20)	1.5 (0.99)	97.3 (0.94)	0.16 (0.03)
142/1/10	6	0.5 (0.22)	0.0 (0.06)	1.1 (0.19)	0.2 (0.19)	71.1 (0.97)	10.7 (0.46)	0.4 (0.17)	11.9 (0.29)	1.9 (0.37)	97.9 (0.41)	0.15 (0.01)
142/1/20	7	0.3 (0.19)	0.0 (0.03)	1.4 (0.15)	0.4 (0.50)	70.6 (1.13)	9.8 (0.55)	0.2 (0.11)	11.2 (0.31)	3.8 (0.31)	97.7 (0.35)	0.14 (0.01)
142/1/40	5	0.3 (0.05)	0.0 (0.04)	1.6 (0.05)	0.6 (0.37)	69.3 (0.86)	10.2 (0.35)	0.2 (0.08)	10.8 (0.16)	3.8 (0.17)	96.7 (0.90)	0.15 (0.01)
142/1/120	6	0.3 (0.18)	0.1 (0.03)	1.6 (0.07)	1.1 (0.72)	68.5 (1.17)	8.8 (0.40)	0.3 (0.08)	10.4 (0.16)	6.0 (0.29)	97.0 (0.60)	0.13 (0.01)
142/2/5	5	0.7 (0.24)	0.1 (0.03)	1.8 (0.49)	0.1 (0.07)	66.7 (1.25)	17.8 (0.84)	0.5 (0.22)	7.7 (0.59)	1.2 (0.44)	96.7 (0.24)	0.27 (0.01)
142/2/20	6	3.3 (2.84)	0.1 (0.04)	2.4 (0.71)	14.2 (17.93)	47.0 (15.24)	16.8 (2.08)	0.2 (0.09)	9.8 (1.65)	3.3 (0.59)	97.0 (1.28)	0.41 (0.18)
142/2/40	3	0.3 (0.08)	0.1 (0.09)	2.7 (0.11)	0.6 (0.61)	65.5 (1.96)	16.3 (1.74)	0.2 (0.12)	8.0 (0.40)	1.9 (0.94)	95.7 (2.51)	0.25 (0.02)
142/2/120	5	0.4 (0.19)	0.1 (0.06)	2.4 (0.32)	2.0 (1.09)	63.9 (1.42)	15.6 (1.60)	0.2 (0.04)	7.7 (1.03)	3.2 (0.52)	95.5 (2.46)	0.24 (0.03)
142/3/40	3	1.6 (1.12)	0.2 (0.06)	7.1 (0.56)	43.4 (6.45)	13.7 (4.92)	21.1 (1.42)	0.2 (0.13)	7.7 (0.24)	0.9 (0.23)	95.9 (1.92)	1.55 (0.59)
142/3/120	2	3.7 (3.52)	0.2 (0.06)	3.7 (0.21)	2.6 (2.05)	53.2 (6.44)	28.1 (2.84)	0.2 (0.10)	4.6 (0.89)	0.6 (0.21)	97.1 (1.61)	0.53 (0.12)
150/1/5	7	0.2 (0.16)	0.1 (0.04)	1.1 (0.13)	0.5 (0.48)	69.6 (1.34)	9.4 (0.29)	0.2 (0.08)	11.1 (0.16)	3.6 (0.31)	95.8 (0.89)	0.14 (0.00)
150/1/120	5	0.2 (0.04)	0.0 (0.03)	1.9 (0.05)	3.3 (0.54)	64.4 (0.61)	9.2 (0.22)	0.3 (0.06)	10.6 (0.21)	4.3 (0.18)	94.4 (0.83)	0.14 (0.00)

n represents the number of spinels analyzed in each experimental charge. Fe_2O_3 and FeO have been calculated by stoichiometry (see Data Reduction). Numbers in parentheses indicate the standard deviation of the analyses performed on a sample. Note that depending on the amount of contamination, NaO, K_2O and CaO may be above their detection limits.

($Fe^{2+}Fe_2^{3+}O_4$), magnesioferrite ($Mg^{2+}Fe_2^{3+}O_4$), trevorite ($Ni^{2+}Fe_2^{3+}O_4$), ulvöspinel ($Fe^{2+}{}_2Ti^{4+}O_4$), hercynite ($Fe^{2+}Al_2^{3+}O_4$), spinel sensu stricto ($Mg^{2+}Al_2^{3+}O_4$), chromite ($Fe^{2+}Cr_2^{3+}O_4$) and magnesiochromite ($Mg^{2+}Cr_2^{3+}O_4$) (Robin et al., 1992). We first calculate proportions of trevorite and ulvöspinel from Ni^{2+}, Ti^{4+}, Fe^{2+} and Fe^{3+} cations, then proportions of magnesiochromite and chromite from Mg^{2+} and Cr^{3+}, and remaining Fe^{2+} and Fe^{3+} cations, proportions of spinel and hercynite from Al^{3+}, and remaining Fe^{2+} and Mg^{2+} cations and finally proportions of magnesioferrite and magnetite from the remaining Mg^{2+}, Fe^{2+} and Fe^{3+} cations.

3. RESULTS

Toppani et al. (2001) have shown that spinel crystallization in the experimental charges is highly dependent on the heating-pulse conditions, i.e., temperature, duration, and oxygen fugacity. For Orgueil samples and over the studied range of oxygen fugacity (log $fO_2 = -0.68$ to -8), spinel crystals occur for temperatures between $\sim$ 1200 and 1500°C and run times between 2 s and 120 s (Table 1). This confirms the very fast kinetics of spinel crystallization and the fact that their occurrence is intimately related to the paired parameters temperature/duration of the heating-pulse (see also fig. 11 in Toppani et al., 2001). For clarity, the colinearity between these two parameters will be expressed by the term τ, which defines the degree of heating of the sample. Qualitatively, high values of τ indicate either a high temperature and/or a long heating-pulse, while low values of τ correspond to low temperature and/or short heating-pulse. In fact, this term can be understood as being

proportional to the melting rate of the sample above ~1200°C. Low τ produces incipient partial melting of the sample during the heating-pulse while high τ results in more extensive melting of the sample.

3.1. Spinel Size and Texture

The sizes of spinels crystallizing during these pulse-heating experiments are in general proportional to τ. For low degrees of melting, at low τ, minute to small size spinels (below 3–4 μm) crystallize at the periphery of the sample (Fig. 1a,b), mimicking the so-called "magnetite shell" surrounding most micrometeorites. Spinels are embedded in an iron-rich melt produced by peripheral partial melting of hydrous iron-rich phases of Orgueil (Toppani et al., 2001). For higher degrees of melting, at higher τ, larger euhedral spinels (up to 10 μm) together with anhydrous silicates crystallize toward the core of the particle from a more homogeneous melt (Fig. 1c). As previously noted (Toppani et al., 2001), this ubiquitous crystallization of spinels with increasing τ leads to the progressive obliteration of the spinel rim (Fig. 1d). We also found that decreasing the oxygen fugacity leads to a smaller size and scarcer occurrence of the spinel crystals (Fig. 1e,f), in agreement with the closure of the magnetite stability field at low fO_2.

3.2. Spinel Composition

Despite the difficulties of probing small size spinels, at least 330 spinels were analyzed for this study, i.e., 2 to 27 spinels per studied sample (Table 2). While some charges show euhedral, dendritic and feathery spinels (Fig. 1d), only euhedral spinels were analyzed for the purpose of this study. For those charges exposed to low τ, spinels were probed exclusively at the near edge of the sample to ascertain as well as possible the continuous reaction of the melt with the imposed atmosphere. For charges heated at a higher τ, location of the spinels in the charge is less important since melting is more complete and equilibration with the atmosphere faster. We tried to limit as much as possible contamination by adjacent phases by probing only the largest crystals in the samples. Nevertheless, it was impossible to circumvent this contamination in charges heated either under reducing conditions (log $fO_2 < -6$, 135/4/20-40; 142/3-40-120 and one of 135/3/40) or at lower temperature (120/2/20), in which only minute spinel crystals are present (~ 1–2 μm).

On the whole, spinels belong to the magnetite (Fe_3O_4)-magnesioferrite ($MgFe_2O_4$) solid-solution series with variable amounts of trevorite ($NiFe_2O_4$), spinel sensu stricto ($MgAl_2O_4$) and hercynite ($FeAl_2O_4$). In detail, they show a large range of composition trending from almost pure magnetite toward the magnesioferrite end-member. Their Al_2O_3 contents reach up to 10 wt%, MgO contents up to 12 wt% and NiO contents up to 6 wt% depending on the experimental conditions. Cr_2O_3, TiO_2 and MnO contents are low, and usually below their detection limits (<0.5 wt%). However, the Cr_2O_3 content of spinel may increase up to ~ 40 wt% in charges heated in a reducing atmosphere for a long duration (e.g., run 142/3/40). The FeO/Fe_2O_3 ratio varies between 0.45 to 0.1. Notice that when the chromium content is high, values of the FeO/Fe_2O_3 ratio may exceed 1 due to substitution of Fe^{3+} by Cr^{3+} in the spinel lattice.

Pure magnetites ($FeO/Fe_2O_3 = 0.45$, with Al_2O_3, MgO and NiO below detection limits) were also probed in this study (Table 2), mainly in the charges processed at low τ (e.g., runs 50/1/20; 800/1/20; 120/1/5; 120/1/10; 120/2/5). These magnetites are framboidal, and/or slightly corroded, and were disregarded for the purpose of this study since they correspond to the pristine magnetite found in the unheated Orgueil material (Nagy and Claus, 1962; Kerridge, 1970; Hyman et al., 1978; Hyman and Rowe, 1983).

3.3. Influence of Oxygen Fugacity, Run Time, and Temperature on Spinel Composition

Due to the short duration of the heating-pulses, spinels in a single charge have heterogeneous compositions with high standard deviations (Fig. 2 and Table 2). However, since these compositional heterogeneities decrease significantly with increasing τ, i.e., the time and/or the temperature of the experiments (Table 2 and Fig. 2), the scattering of the spinel compositions in each charge is hereafter expressed by the arithmetic mean of spinel compositions plus or minus one standard deviation. Some uncertainties still remain because (1) a shift may exist between spinel chemical evolution deduced from these arithmetic means and that obtained from a more robust statistical treatment of our data set (Fig. 2) and (2) some compositional heterogeneity may be introduced by the necessity of using different chips of Orgueil as starting material for each run. Nevertheless, we consider that our set of experiments and their representation by their arithmetic means allows a good evaluation of the effects of the duration, the temperature, and the oxygen fugacity of the heating-pulses on the spinel composition.

3.3.1. Influence of Time

For a fixed oxygen fugacity ($\log fO_2 = -0.68$) and different temperatures, Al_2O_3 (Fig. 3a), NiO (Fig. 3b) and MgO (Fig. 3c) contents of spinels all increase while their FeO/Fe_2O_3 ratios decrease with the duration of the heating-pulses (Fig. 3d). Table 2 shows that these trends are also valid for other oxygen fugacities. In addition, these experiments reveal that, for very short heating times (<2–3 s), Al_2O_3 and NiO contents are below detection limits in contrast with MgO that still remains in appreciable amounts. Interestingly, both Al_2O_3 contents and FeO/Fe_2O_3 ratios of spinels level off for the longest run durations (Figs. 2 and 3a,d, and Table 2).

3.3.2. Influence of Oxygen Fugacity

Changes in oxygen fugacity also significantly affect the spinel composition. For instance, decreasing the oxygen fugacity results in an increase of both the FeO/Fe_2O_3 ratio and the Al_2O_3 content of the spinel and a decrease of the MgO content (Table 2). The behavior for NiO seems, however, more variable.

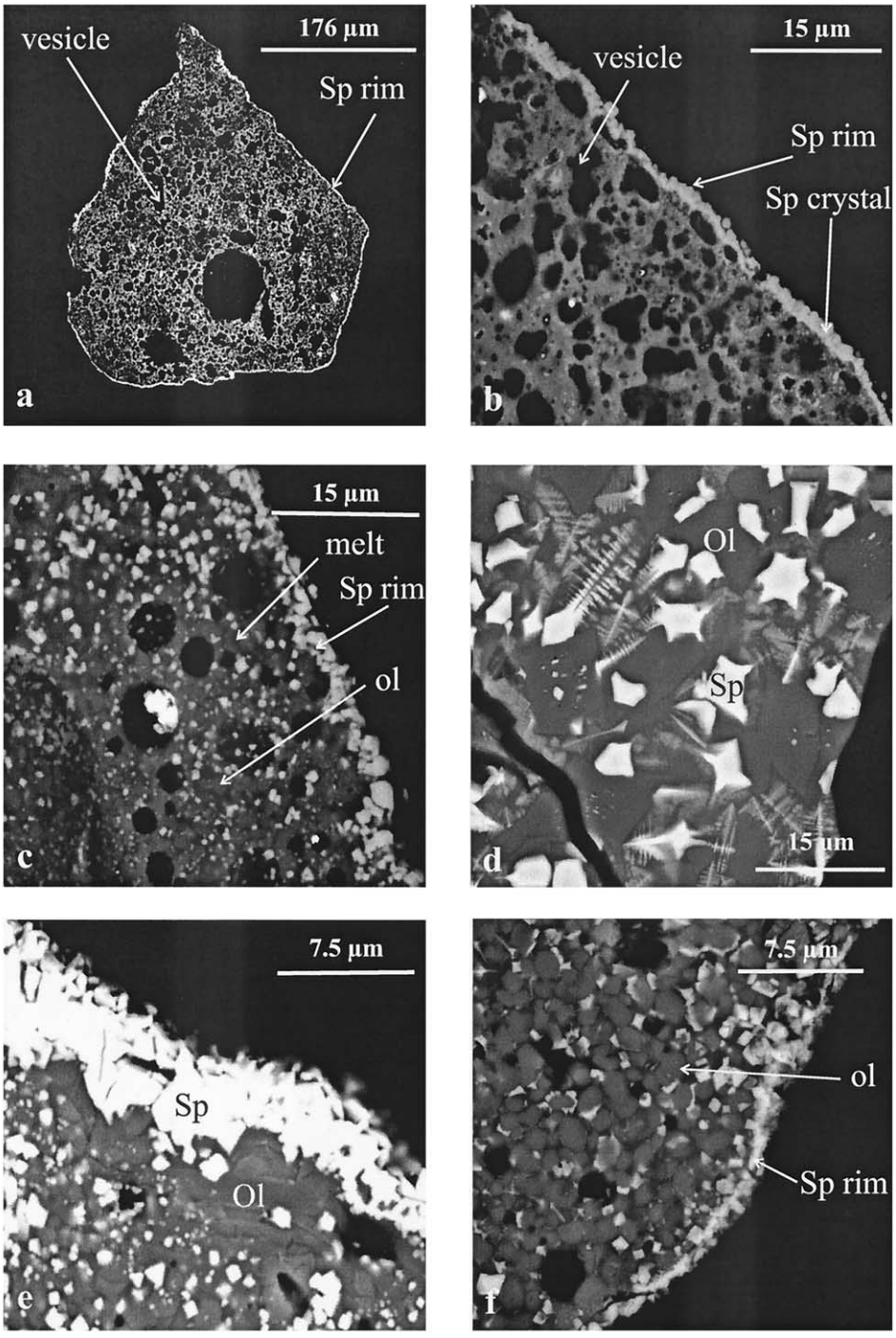

Fig. 1. Backscattered electron images of polished sections of representative pulse-heated Orgueil fragments showing the effects of temperature, run time and oxygen fugacity on their textures.

Experimental charges heated at different temperatures and times showing the effect of increasing degree of heating (a–d): (a) 1350°C, for 5 s, under log $fO_2 = -3.26$ (run 135/2/5, see Table 1), (b) 1350°C, for 5 s, under log $fO_2 = -3.26$ (detail of the periphery of the same run 135/2/5), (c) 1350°C, for 10 s, under log $fO_2 = -3.26$ (run 135/3/10), (d) 1425°C for 120 s under log $fO_2 = -3.27$ (run 142/2/120). The fragment heated for 5 s (a, b) shows numerous vesicles related to dehydration and is surrounded by a well-defined spinel rim. Fragment (c), heated for 10 s, shows clear evidence of partial melting with recrystallization of spinels (sp) and anhydrous silicates (olivine:ol) inward and a spinel rim thicker than in (a, b). Fragment (d) shows large olivines and both euhedral and dendritic spinels in a glassy mesostasis. Notice that the homogenization of the texture from a to d leads to the disappearance of the spinel rim.

Experimental charges heated at the same temperatures and times showing the effect of oxygen fugacity: (e) 1350°C for 20 s under log $fO_2 = -3.26$ (run 135/2/20), (f) 1350°C for 20 s under log $fO_2 = -8$ (run 135/4/20). Note that the size and the abundance of spinel decrease with the fO_2.

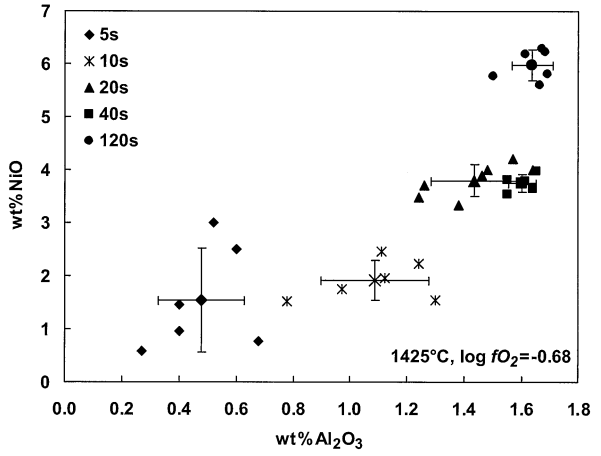

Fig. 2. Concentration in NiO versus Al_2O_3 of spinels measured in five experimental charges heated at 1425°C, under log $fO_2 = -0.68$ for different run times (from 5–120 s) showing the compositional heterogeneity of spinels belonging to a single charge as a function of the heating time. Symbols with error bars (standard deviation − 1σ) represent the mean composition of spinels belonging to a single charge. Notice that spinel composition trends toward homogeneity with time.

3.3.3. Influence of Temperature

Our results (Table 2 and Fig. 3) show that Al_2O_3, NiO and MgO concentrations of spinels increase with temperature and that these enrichments are thermally activated. For instance, enrichment in Ni or Al of spinels is more rapid at 1425°C than for temperatures of 1350°C or 1200°C. Since these effects mimics those obtained for different run durations at fixed temperature, this feature illustrates that both temperature and time produce the same effects on the spinel composition.

4. COMPARISONS BETWEEN SYNTHETIC AND COSMIC SPINELS

4.1. Comparison with Cosmic Spinel Morphology

Our experiments reproduce most of the morphology of the spinels formed during the atmospheric entry of extraterrestrial objects such as some micrometeorites, cosmic spherules or fusion crusts of stony meteorites.

Experimental spinels synthesized at low τ (135/1/10, 120/2/20, 142/2/5; Table 1), resemble peripheral spinels of fine-grained MMs or scoriaceous MMs (Genge et al., 1997; Kurat et al., 1994), whereas those obtained at high τ (135/1/40, 142/1/10, 142/2/40, 150/2/10; Table 1), are similar to spinels found in some cosmic spherules or meteorite fusion crusts (Brownlee and Bates, 1983; Genge and Grady, 1999). Figures 4a, b, c and d show spinels from a fine-grained MM, a scoriaceous MM, a cosmic spherule and the Orgueil fusion crust respectively. Comparison between Figure 1 and Figure 4 allows similarities between experimental and cosmic spinels to be underlined.

The most plausible mechanism for the formation of the

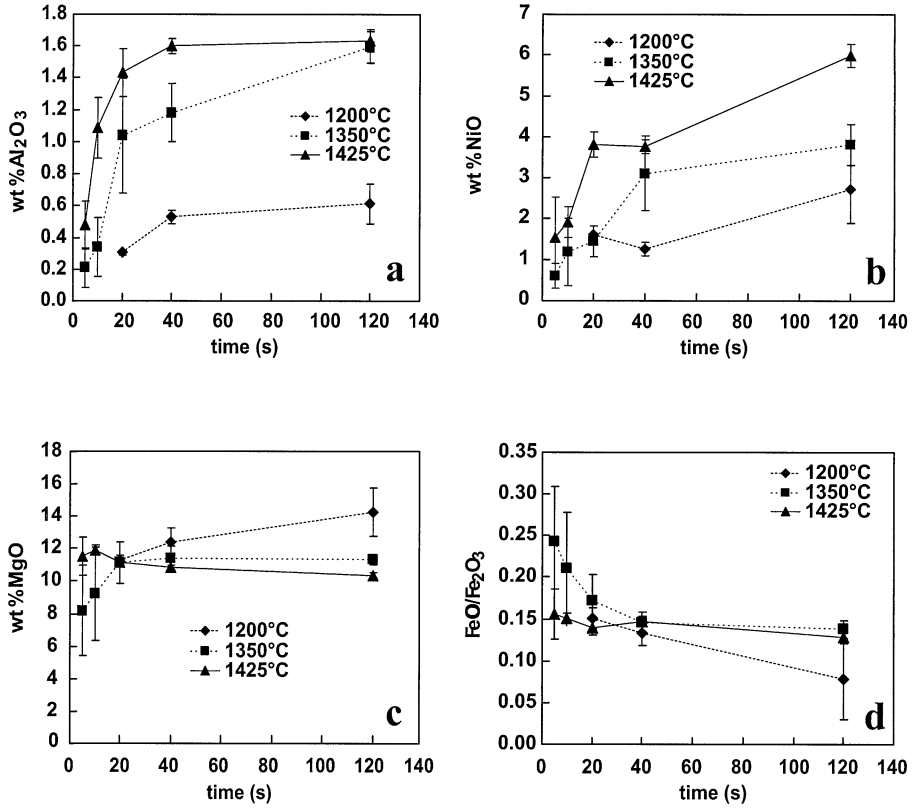

Fig. 3. Average concentrations of (a) Al_2O_3 (b) NiO and (c) MgO and of (d) the FeO/Fe_2O_3 ratio of spinels analyzed in charges heated under log $fO_2 = -0.68$ at different temperatures and for different run times (see text for discussion).

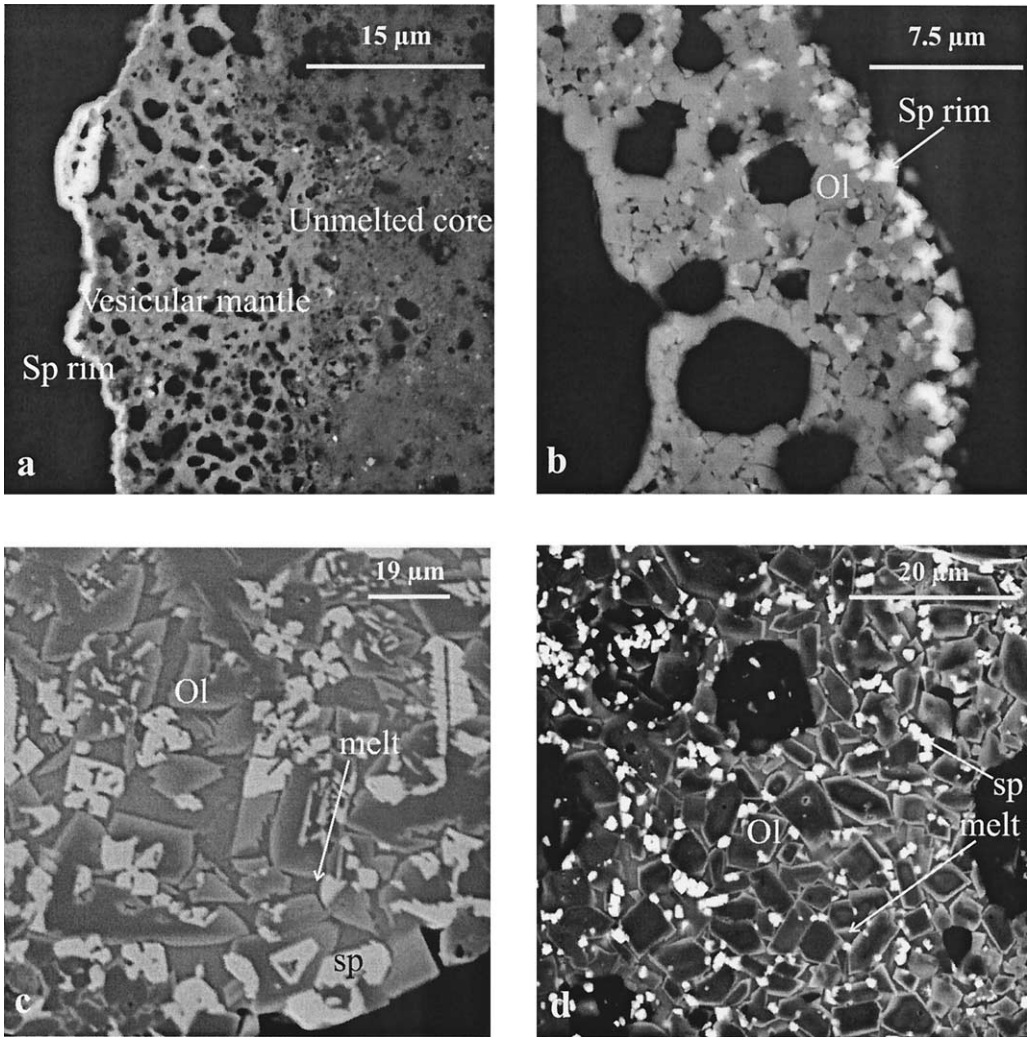

Fig. 4. Backscattered electron images of polished sections of MMs and Orgueil fusion crust: (a) periphery of a fine-grained MM, (b) periphery of a scoriaceous MM, (c) periphery of a cosmic spherule, (d) outer part of the fusion crust of Orgueil. The fine-grained MM (a) shows a spinel rim, a vesicular mantle and an unmelted core. The scoriaceous MM (b) shows well-defined spinel and olivine crystals. Both the cosmic spherule (c) and the fusion crust of Orgueil (d) show an homogeneous texture of recrystallization of olivines and spinels. Note that the cosmic spherule (c) shows both euhedral and dentritic spinels.

cosmic spinels is thus the partial melting of the host objects during their entry in the Earth's atmosphere and the subsequent crystallization of spinels. The formation of a spinel rim on fine-grained and scoriaceous MMs is very likely related to peripheral partial melting of iron-rich ferrihydrite and/or phyllosilicate phases due to an elevated radial thermal gradient inside the particle, leading to the formation of an iron-rich melt (Toppani et al., 2001). Because of its low saturation level, spinel becomes rapidly oversaturated in this melt, resulting in its rapid crystallization at the periphery of the sample. The higher degree of heating observed in the outer fusion crust of most meteorites (Ramdohr, 1967; Fruland, 1974; Genge and Grady, 1999) or in cosmic spherules (Brownlee and Bates, 1983; Genge et al., 1997; Engrand and Maurette, 1998) leads to more prominent melting and ubiquitous crystallization of spinels (Fig. 4) which, in turn, explains the obliteration of the spinel rim at the periphery of these objects.

4.2. Comparison with Cosmic Spinel Composition

To enlarge as much as possible the literature data set on cosmic spinel compositions, we analyzed more than 130 new spinels (Table 3) from: 3 fine-grained MMs, 1 intermediate fine-grained/scoriaceous MM, 5 scoriaceous MMs and 6 cosmic spherules belonging to the French MMs collection (CSNSM, Orsay). As with the experimental charges, only spinels of sufficient size were probed in these extraterrestrial objects, excluding for instance, the tiniest spinels from the nonvesicular fine-grained MMs. In addition, spinels from fine-grained and scoriaceous MMs (low τ) were probed at the periphery of the objects whereas spinels were probed independently of their location in cosmic spherules (high τ). Cosmic spinels from any MMs or cosmic spherules are in general very heterogeneous in composition, likely due to the occurrence of zonation.

Table 3. Average compositions of spinels analyzed in micrometeorites and cosmic spherules from the French MMs collection

Sample designation[a]	Sample description	n	SiO_2	TiO_2	Al_2O_3	Cr_2O_3
92-17/5	NV fg	8	1.0 (0.84)	0.5 (0.60)	0.7 (0.33)	0.2 (0.17)
94-4b/11	V fg	16	0.7 (0.42)	0.0 (0.04)	0.5 (0.12)	0.1 (0.05)
94-4b/28	V fg	4	0.2 (0.14)	0.0 (0.01)	0.4 (0.02)	0.0 (0.03)
94-4b/46	fg-sc	6	0.5 (0.29)	0.0 (0.02)	0.3 (0.11)	0.0 (0.03)
99-24/52	sc	6	0.8 (0.27)	0.3 (0.18)	1.7 (0.66)	1.8 (1.37)
94-4b/7	sc	4	0.6 (0.73)	0.0 (0.04)	0.5 (0.35)	0.1 (0.07)
99-24/38	sc	7	0.8 (0.73)	0.1 (0.05)	0.5 (0.18)	0.1 (0.09)
96-18/1	sc	7	1.0 (0.70)	0.1 (0.04)	1.5 (0.85)	0.3 (0.16)
92-17/3	sc	6	0.9 (0.44)	0.0 (0.03)	1.1 (0.22)	0.1 (0.05)
96-1/9	cs	14	0.7 (0.27)	0.5 (0.09)	5.3 (0.40)	1.7 (1.58)
96-1/21	cs	20	0.8 (0.45)	0.1 (0.05)	2.6 (0.32)	0.7 (0.89)
96-1/16	cs	9	0.8 (0.31)	0.4 (0.08)	5.1 (0.43)	2.3 (2.14)
96-17/2	cs*	9	0.5 (0.34)	0.1 (0.05)	2.3 (0.31)	1.7 (0.80)
96-17/6	cs	8	0.4 (0.09)	0.2 (0.08)	3.7 (0.37)	1.0 (1.24)
96-21/1	cs**	7	1.1 (0.59)	0.1 (0.06)	4.0 (0.20)	1.4 (0.74)

Sample description: NV fg, no-vesicular fine-grained MM; V fg, vesicular fine-grained MM; sc, scoriaceous MM; cs, cosmic spherule. n represents the number of spinels analyzed in each sample. Fe_2O_3 and FeO have been calculated by stoichiometry (see § data reduction). Numbers in parentheses indicate the standard deviation of the analyses performed on a sample.

* Bubbling cosmic spherule.

** Bubbling cosmic spherule with large anhydrous crystals embedded in glass.

Besides reproducing the morphology of most of the cosmic spinels, these experiments were also able to reproduce the main chemical features of the cosmic spinels (Table 3; Robin et al., 1992; Kurat et al., 1994). As was true for experimental spinels, cosmic spinels present a large range of both Fe^{2+}/Fe^{3+} ratios and of Al, Mg or Ni contents with low chromium contents in most cases. This similarity is further illustrated in Figure 5, in which the scattering of synthetic spinels matches almost perfectly that of cosmic spinels, in terms of the three end-members: magnetite, magnesioferrite and spinel. In addition, cosmic spinel compositions can be related to the types of extraterrestrial objects in which they occur. For instance, magnetite is the dominant end-member in spinels from MMs, whereas magnesioferrite is the major component of spinels from meteorite fusion crusts. Cosmic spinels, and their experimental analogues are therefore different from their terrestrial counterpart (Haggerty, 1976; Robin et al., 1992), since most common terrestrial spinels contain very low amounts of magnesioferrite and trevorite ($NiFe_2O_4$). While beyond the scope of this study, these main differences between terrestrial and cosmic spinels (Robin et al., 1992) very likely reflect differences in both bulk compositions of the crystallizing material and conditions of formation.

5. MODELING OF THE SPINEL COMPOSITIONAL EVOLUTION

Since our synthesized spinels match several characteristics observed in cosmic spinels and seem therefore relevant to their study, we will now use our experimental results to understand the factors that control spinel composition and its variability.

5.1. Factors Controlling Synthetic Spinel Composition

5.1.1. FeO/Fe_2O_3 Ratio

Since the ferrous/ferric ratio of spinels depends on several parameters, we look first at spinel compositions obtained in the longest runs. Figure 6a represents the FeO/Fe_2O_3 ratio of

Table 3. (Continued)

Fe_2O_3	FeO	MnO	MgO	NiO	Total	FeO/Fe_2O_3
64.1 (2.70)	22.9 (1.75)	0.2 (0.10)	3.9 (0.93)	2.9 (0.79)	96.5 (0.48)	0.36 (0.04)
65.0 (1.61)	25.4 (1.80)	0.2 (0.09)	3.0 (1.04)	0.5 (0.19)	95.4 (2.01)	0.39 (0.02)
66.8 (0.90)	23.8 (0.80)	0.5 (0.06)	3.2 (0.64)	0.7 (0.35)	95.5 (0.46)	0.36 (0.02)
64.3 (2.11)	22.2 (1.47)	0.3 (0.16)	4.1 (1.08)	0.6 (0.09)	92.2 (2.13)	0.35 (0.02)
61.6 (3.17)	20.9 (4.80)	0.2 (0.09)	4.5 (3.55)	3.2 (0.45)	94.8 (0.88)	0.34 (0.09)
62.1 (2.90)	25.4 (2.11)	0.1 (0.07)	2.1 (0.33)	0.5 (0.20)	91.3 (5.81)	0.41 (0.02)
64.2 (1.40)	29.8 (0.97)	0.1 (0.10)	0.7 (0.34)	0.2 (0.11)	96.4 (1.85)	0.45 (0.18)
63.5 (2.34)	22.3 (0.83)	0.3 (0.12)	3.9 (0.64)	2.9 (0.85)	95.7 (1.04)	0.35 (0.01)
62.7 (1.68)	26.8 (0.72)	0.1 (0.06)	1.8 (0.47)	1.2 (0.33)	94.8 (1.85)	0.43 (0.01)
58.5 (1.44)	25.8 (1.57)	0.3 (0.11)	3.7 (0.80)	0.8 (0.57)	97.3 (2.24)	0.44 (0.02)
65.8 (1.52)	23.9 (1.82)	0.1 (0.05)	3.0 (0.55)	3.5 (0.60)	97.2 (2.07)	0.38 (0.03)
59.2 (2.77)	26.4 (1.74)	0.1 (0.07)	3.2 (0.71)	1.7 (0.59)	99.1 (1.03)	0.45 (0.03)
64.2 (2.00)	25.3 (2.41)	0.3 (0.11)	3.4 (0.91)	1.0 (0.32)	98.9 (1.99)	0.40 (0.04)
61.7 (1.95)	24.0 (1.64)	0.1 (0.07)	4.0 (0.82)	1.0 (0.33)	96.1 (0.52)	0.39 (0.03)
61.0 (1.60)	22.4 (1.76)	0.2 (0.05)	5.4 (0.65)	1.6 (0.32)	97.2 (0.88)	0.37 (0.03)

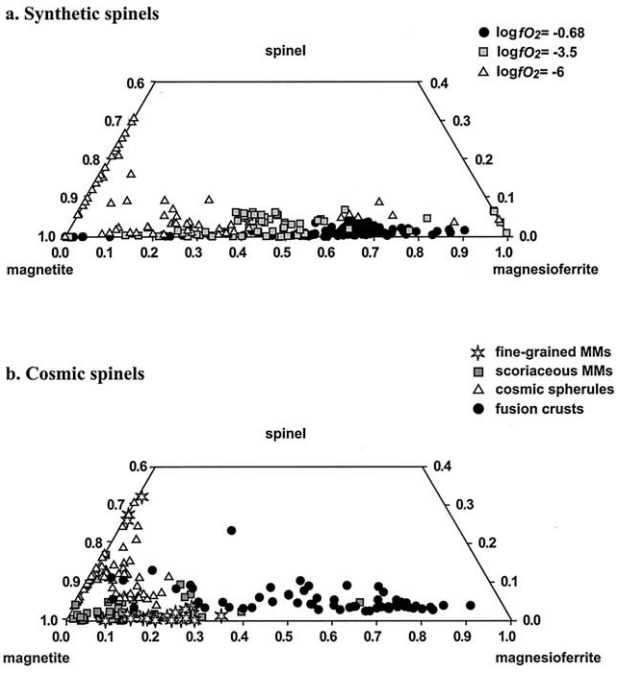

Fig. 5. Comparisons of composition between synthetic and cosmic spinels in magnetite (Fe_3O_4)-magnesioferrite ($MgFe_2O_4$)-spinel ($MgAl_2O_4$) ternary plots. Note the similarities of compositional fields between (a) spinels having crystallized in the experimental charges (data given as a function of fO_2 for various temperatures and run times) and (b) cosmic spinels from fine-grained MMs, scoriaceous MMs, cosmic spherules and fusion crusts of meteorites (Table 3). Composition of spinels from fusion crusts were measured in Allende, Aumale, Orgueil and Saint-Séverin chondrites (Robin, personal communication).

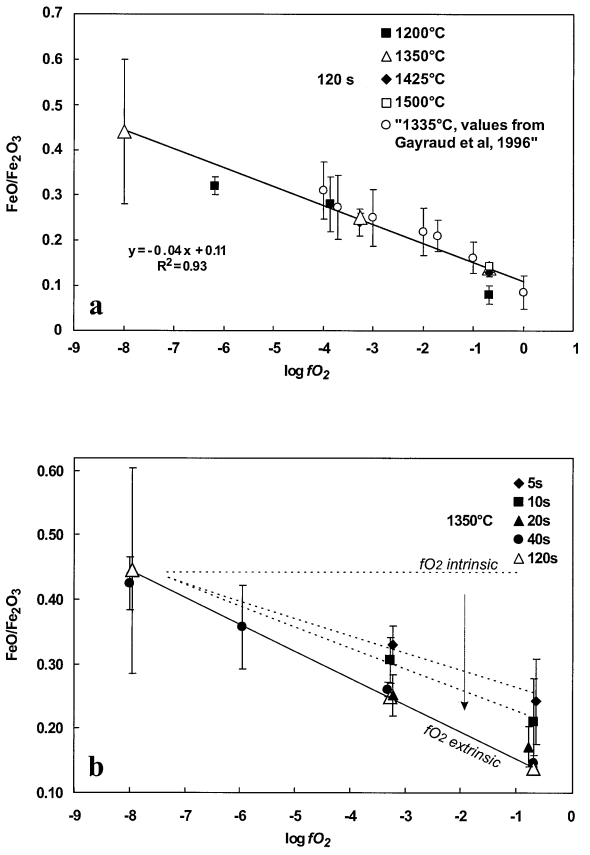

Fig. 6. (a) Mean values of the FeO/Fe_2O_3 ratio of spinels as a function of the oxygen fugacity at equilibrium (charges heated for run times of 120 s). Notice that large error bars may be due to either contamination or a small number of spinel analyses (see Table 2). Straight line corresponds to the regression line of this data set. (b) Variation of the mean FeO/Fe_2O_3 ratio of the spinels analyzed in charges heated at 1350°C for different run times and oxygen fugacities. Solid lines correspond to near equilibrium conditions (~120 s) while dashed lines show the evolution of the spinel FeO/Fe_2O_3 ratio as a function of time (see text for explanation).

spinels crystallized in charges heated for 120 s under different fO_2 and various temperatures (1200, 1350, 1425 and 1500°C). Data from the study of Gayraud et al. (1996), obtained on spinels analyzed in Orgueil charges heated at 1335°C for 120 s under variable fO_2, were also added. Besides demonstrating the good agreement between these two experimental studies, this graph shows that, for such heating-pulse durations, the FeO/Fe_2O_3 ratio of spinels increases linearly as the logarithm of the oxygen fugacity decreases from −0.68 and −8, and is independent of temperature in the range of 1200–1500°C. Since similar relationships for spinels were obtained from basaltic equilibrium crystallization experiments by Hill and Roeder (1974), Fisk and Bence (1980), and Maurel and Maurel (1984), we conclude that heating times of ~120 s allow the ferrous/ferric ratio of spinels to approach the values expected for equilibrium conditions. This is further supported by the leveling off of the FeO/Fe_2O_3 ratios of spinels for the longest run durations (Figs. 2 and 3d, and Table 2) as well as by results from an experiment performed at 240 s (Table 2, run 135/2/240). Furthermore, experiments performed on both basaltic and chondritic compositions (Hill and Roeder, 1974; Gayraud et al., 1996) have shown that the ferrous/ferric ratio of spinels is independent of the melt composition and controlled only by the oxygen fugacity. From this, we suggest that, at near equilibrium conditions (~120 s) the FeO/Fe_2O_3 ratio of spinels depends solely on the imposed oxygen fugacity.

If the FeO/Fe_2O_3 ratio of spinels from samples heated at 1350°C for different run times is plotted as a function of fO_2 (Fig. 6b), one can see that, at fixed extrinsic fO_2 (the imposed furnace atmosphere) and temperature, the spinel FeO/Fe_2O_3 ratio varies with time. For instance, under an extrinsic log fO_2 = −0.68, the spinel FeO/Fe_2O_3 ratio evolves from a value of 0.24 for t = 5 s to the equilibrium value of 0.14 for t = 120 s (Fig. 6b). A similar trend is observed for log fO_2 = −3.26, while for more reduced conditions, this FeO/Fe_2O_3 ratio variation narrows, until at log fO_2 = −8 the FeO/Fe_2O_3 ratio is constant with time (FeO/Fe_2O_3 ratio ~ 0.45). This suggests that, in the studied range of oxygen fugacities and for a given temperature, the FeO/Fe_2O_3 ratio of spinels evolves with time, for a given extrinsic fO_2, from an initial value to its equilibrium value, recording thus the evolution of the instantaneous redox state of the melts produced by the partial melting of Orgueil. In others words, this means that, because of its rapid kinetics of crystallization, the spinel records, through its FeO/Fe_2O_3 ratio, the instantaneous oxidation state of the melt from which it crystallizes.

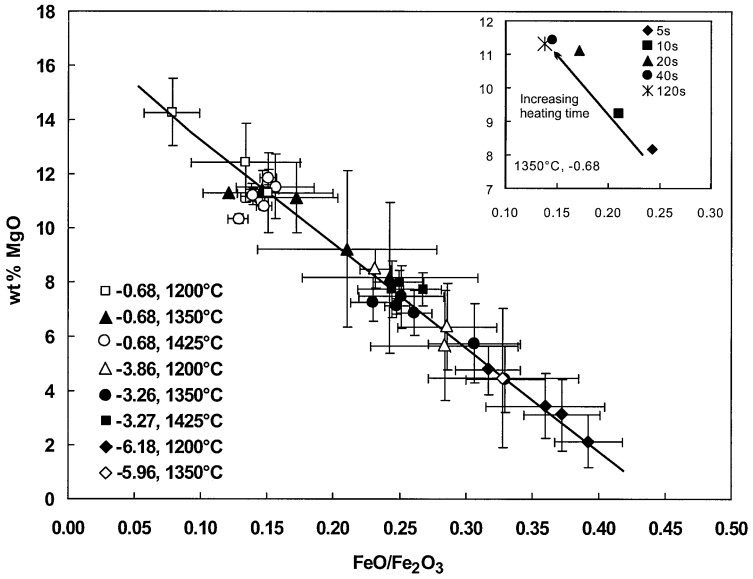

Fig. 7. Means of the MgO content versus FeO/Fe_2O_3 ratio of spinels analyzed in charges heated at different temperatures and oxygen fugacities for various run times. The plot inserted in the top-right corner is a close-up view of the spinels analyzed in the charges heated at 1350°C under log $fO_2 = -0.68$ for different run times.

The initial value was set at $FeO/Fe_2O_3 = 0.45$ (± 0.02) because preferential partial melting of ferrihydrite and other iron-rich hydrous minerals (Toppani et al., 2001) produces early melts that are iron-oversaturated and impoverished in silica and in all the remaining elements, favoring the crystallization of an almost pure magnetite ($FeO/Fe_2O_3 = 0.45$). This choice is supported by the Al_2O_3, NiO and MgO poor compositions of the first spinels crystallizing during short heating-pulses (Table 2, and Fig. 3). This feature is well illustrated in Figure 7 which shows that spinel MgO content is anticorrelated with FeO/Fe_2O_3 ratio for charges heated at different temperatures, run times and oxygen fugacities. As shown in the closer view, the MgO content of spinel decreases with run time. Extrapolation of this linear trend back to t = 0 s (MgO wt% = 0) demonstrates that the first spinels to crystallize have a fixed FeO/Fe_2O_3 ratio close to that of pure magnetite ($FeO/Fe_2O_3 = 0.45$).

These spinel FeO/Fe_2O_3 ratio trends are similar for the different studied temperatures (see Table 2) though they are less resolvable at the highest temperatures (1425–1500°C), due to the thermal activation of the process.

Therefore, in these pulse-heating experiments on Orgueil material, the FeO/Fe_2O_3 ratio of spinels from charges heated at a given temperature and oxygen fugacity varies with time from an initial ratio of 0.45 to an equilibrium value imposed by the extrinsic oxygen fugacity. This value of 0.45 could be understood as the spinel FeO/Fe_2O_3 ratio imposed at t = 0 s by the intrinsic oxygen fugacity of the Orgueil material, which by comparison with our experimental data may correspond to a log $fO_2 \cong -8$.

5.1.2. *Aluminum*

As was true for the FeO/Fe_2O_3 ratio, the spinel Al content levels off as a pulse-heating time of 120 s is approached, suggesting that near equilibrium conditions have been reached. At near equilibrium conditions (~120 s), the spinel Al content correlates negatively with the extrinsic oxygen fugacity (Fig. 8, this study, and Gayraud et al., 1996). This trend is consistent with an increase in the Fe^{2+}/Fe^{3+} of the melt and the correlative substitution of Al^{3+} for Fe^{3+} in the spinel lattice with decreasing oxygen fugacity (Hill and Roeder, 1974). On average, the Al content of spinels is positively correlated with the temperature of the heating-pulse. Nevertheless, it is noticeable that the higher the temperature, the more negative the correlation with the extrinsic oxygen fugacity (see below).

For conditions out of equilibrium (t < 120 s), the Al content of spinels varies from almost 0 wt% to near equilibrium values (see, e.g., Fig. 3, Fig. 8 or Table 2), and its behavior is overwhelmingly dominated by the parameter τ of the pulse-heating experiments. Since Al is mainly hosted in the phyllo-

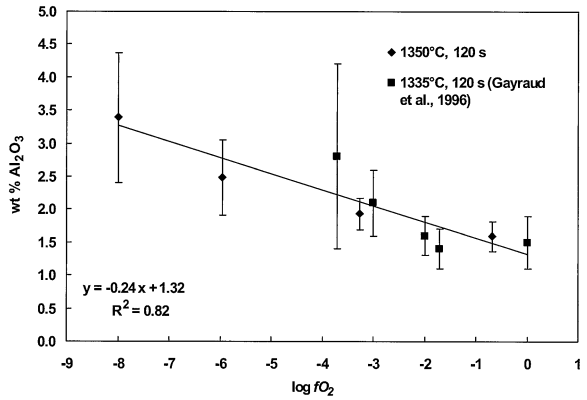

Fig. 8. Means of the Al_2O_3 content of spinels analyzed in charges heated at 1350°C for long run time (120 s) under different oxygen fugacities. For log $fO_2 = -6$, we have used the Al_2O_3 content of spinels of a charge heated during 40 s because of the high Cr_2O_3 content of the spinels of the charge heated during 120 s.

silicate matrix of Orgueil material (Tomeoka and Buseck, 1988), this aluminum increase can be related to changes in the melt composition (see also Maurel and Maurel, 1982a, 1983), as the rate of Orgueil material partial melting increases due to the increase of τ. Even if oxygen fugacity may affect the aluminum content of the spinels, this effect must be minor since Al content of spinels should decrease with increasing run times as the fO_2 increases from the intrinsic to the extrinsic fO_2. We consider that the Al_2O_3 content of spinels in such pulse-heating experiments mainly depends on the aluminum content of the melt and therefore on the melting rate of the sample. This feature is further supported by the incompatible behavior of Al in the cocrystallizing phases (olivine and low-Ca pyroxenes), which may explain the relatively stable behavior of Al as a function of parameter τ (Fig. 3 and Table 2).

5.1.3. Magnesium and Nickel

As already noticed, Mg and Ni contents of spinels are highly variable and on average, less constrained than Al (Table 2). Two main reasons can be invoked: (1) Ni-bearing phases are numerous and not evenly distributed in the Orgueil starting material (presence of Fe-Ni sulfides and sulfates; Böstrom and Fredriksson, 1966; Kerridge et al., 1979; Tomeoka and Buseck, 1988), and (2) Mg and Ni are highly compatible elements not only in spinels but also in the cocrystallizing silicate phases. Nevertheless, at near equilibrium conditions (~120 s), both Mg and Ni contents of spinels decrease with decreasing oxygen fugacity in agreement with the replacement of Mg^{2+} and Ni^{2+} by Fe^{2+} due to the increase in the Fe^{2+}/Fe^{3+} ratio (Hill and Roeder, 1974). Under nonequilibrium conditions (<120 s), it is almost impossible to decipher the factors that controls Mg and Ni contents of spinels, because of the colinear effects of several of these factors (e.g., increasing content of Mg with fO_2 and parameter τ; see Fig. 7) and of the partitioning of these elements between the different crystalline phases.

5.1.4. Chromium

If, in most of the charges, chromium is below the detection limit, Table 2 shows however that its content may increase significantly in spinel crystallized from charges heated under reducing conditions and for long heating-times. In this range of oxygen fugacity (Schreiber and Haskin, 1976), chromium behaves in a similar manner to aluminum. Under near equilibrium conditions (~120 s), its behavior is dictated by the oxygen fugacity, with an increase in Cr^{3+} of the spinel with increasing Fe^{2+}/Fe^{3+} ratio of the melt (Maurel and Maurel, 1982b). Interestingly, Gayraud et al. (1996) have shown that the Cr content of spinels is also dependent on spinel modal proportions, which may also help to explain the fact that chromiferous spinels are preferentially found in the longest or the most reduced experiments in which spinel crystals are scarce.

5.2. Spinel Modeling

The Al_2O_3 contents and FeO/Fe_2O_3 ratios of spinels are the best constrained compositional parameters and vary in an unequivocal manner with the physical parameters of these experiments. Therefore, both may be used to model the changes of spinel composition in the range of our experimental conditions. We have shown that (1) for a given temperature, the FeO/Fe_2O_3 ratio of spinels of the flash-heated charges depends on the instantaneous fO_2 of the melt which evolves with time from an initial value to the extrinsic fO_2 imposed by the atmosphere, and that (2) the Al_2O_3 content of spinel is mainly controlled by the parameter τ and by the extrinsic fO_2 for values at equilibrium. Because of its rapid crystallization kinetics, we suggest that the spinel, through its Al_2O_3 content and FeO/Fe_2O_3 ratio, provide information about the heating conditions undergone by a sample during a heating-pulse. To obtain such information, it is necessary to model the isothermal evolution of the FeO/Fe_2O_3 ratio and Al_2O_3 content as a function of time and fO_2. The following section presents an example for the 1350°C isotherm.

5.2.1. FeO/Fe_2O_3 Ratio

Knowing the FeO/Fe_2O_3 ratio of spinels at near equilibrium conditions (~120 s) (Fig. 6a) and its variation with the extrinsic oxygen fugacity (Fig. 6b), the kinetic evolution of this ratio can be approximated by an Avrami type equation:

$$y = 1 - \exp(-kt)^n \quad (1)$$

where $y \in [0;1]$ represents the transformed fraction, defined as follows:

$$y = \frac{(FeO/Fe_2O_3)_{ini} - (FeO/Fe_2O_3)_t}{(FeO/Fe_2O_3)_{ini} - (FeO/Fe_2O_3)_{eq}} \quad (2)$$

with k the reaction rate constant, t the time, and n a power law function. In Eqn. 2, $(FeO/Fe_2O_3)_{ini}$ stands for the ferrous/ferric ratio of spinels crystallizing at t = 0 s under the initial fO_2, i.e., $(FeO/Fe_2O_3)_{ini} = 0.45$; $(FeO/Fe_2O_3)_{eq}$ for the ferrous/ferric ratio of spinels crystallizing at near equilibrium conditions (~120 s) under the extrinsic fO_2, and $(FeO/Fe_2O_3)_t$ for the ferrous/ferric ratio of spinels crystallizing at time t s. According to Eqn. 2, the kinetic evolution of the spinel FeO/Fe_2O_3 ratio depends not only on the duration of the pulse but also on the difference between the extrinsic and the initial fO_2. This equation could also be written as:

$$(FeO/Fe_2O_3)_t = 0.45 - [(0.45 - (FeO/Fe_2O_3)_{eq}) \times (1 - \exp(-kt)^n)] \quad (3)$$

According to the Avrami method, $a \ln[-\ln(1 - yr)]$ versus time plot allows the determination of $k \sim 0.209$ and $n \sim 0.618$ parameters. Figure 9a depicts the results of this fit (Eqn. 1) and shows how this model tightly reproduces the 1350°C experimental values.

5.2.2. Al_2O_3 Content

We have also modeled the isothermal evolution (T = 1350°C) of the spinel Al content as a function of time and extrinsic fO_2. The kinetic evolution of the Al content of the synthetic spinel is given in Figure 9b where the ratio $(Al_2O_3)_t/(Al_2O_3)_{eq}$ is plotted as a function of time. In this ratio, $(Al_2O_3)_t$ corresponds to the average Al content of spinels crystallized in a charge heated at 1350°C during t s at a given fO_2, and $(Al_2O_3)_{eq}$ stands for the Al_2O_3 content of spinels crystallized

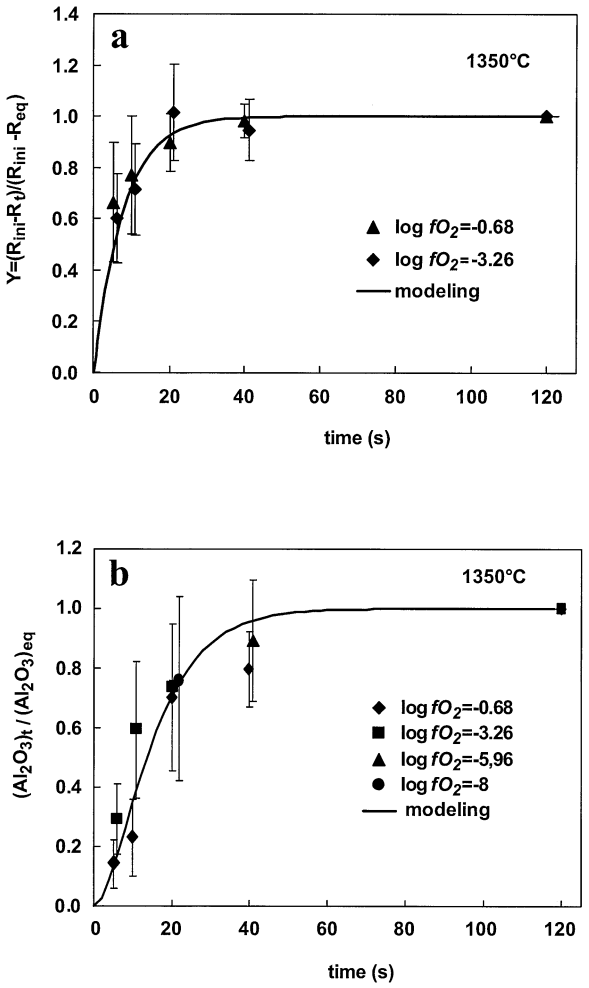

Fig. 9. Kinetic evolution of (a) the FeO/Fe_2O_3 ratio and (b) the Al_2O_3 content of spinels of charges heated at 1350°C for different oxygen fugacities. Symbols represent experimental data while the solid line represents the model described by Eqn. 3 and Eqn. 5 respectively (see text). In plot (a), $Y = \dfrac{R_{ini} - R_t}{R_{ini} - R_{eq}}$ and $R = FeO/Fe_2O_3$.

from a charge heated at 1350°C at the same oxygen fugacity and at near equilibrium conditions. This graph shows clearly that the evolution of the $(Al_2O_3)_t/(Al_2O_3)_{eq}$ ratio is independent of the fO_2 as this dependence is taken into account by both the numerator and denominator of the ratio. To model the Al behavior of spinels crystallizing during such pulse-heating experiments, a first order kinetic equation $y = a\exp(-kt)$ was also used and divided into two successive reactions that involve first, the melting of Orgueil material and the aluminum release into the melt phase (with a rate constant: k_1), and then, the incorporation of Al in the spinel structure (with a rate constant: k_2). The equation is the following:

$$\frac{(Al_2O_3)_t}{(Al_2O_3)_{eq}} = 1 - \left[\frac{k_2}{k_2 - k_1}\exp(-k_1 t)\right] + \left[\frac{k_1}{k_2 - k_1}\exp(-k_2 t)\right] \quad (4)$$

which may be rewritten as follows after the determination of k_1 and k_2,

$$\frac{(Al_2O_3)_t}{(Al_2O_3)_{eq}} = 1 - [1.91\exp(-0.11t)] + [0.91\exp(-0.23t)] \quad (5)$$

The result of this modeling is shown in Figure 9b together with the experimental data obtained for the 1350°C isotherm.

5.2.3. Al_2O_3 Versus FeO/Fe_2O_3 Diagram

Based on these models (depicted in Figs. 6a, 8, and 9), it is now possible to compute the composition (Al_2O_3 and FeO/Fe_2O_3) of any spinel crystallizing in a 1350°C pulse-heating experiment at run times between 0 and 120 s and extrinsic log fO_2 between −0.68 to −8. The results of this modeling are plotted in a Al_2O_3 versus FeO/Fe_2O_3 diagram (Fig. 10a). The bold lines, called hereafter isofugacity-lines, represent the chemical evolution of spinels crystallizing for different run times at a given extrinsic fO_2, and the regular lines, or isotime lines, give the composition of spinels crystallizing at fixed heating-times under different fO_2. In such an isothermal graph, the oxygen fugacity decreases with FeO/Fe_2O_3 ratio along the x-axis whereas heating time increases with Al_2O_3 content along the y-axis. The computation are subject to caution for log $fO_2 < -8$ since in this range of oxygen fugacity (1), the extrinsic oxygen fugacity becomes more reducing than the intrinsic oxygen fugacity of Orgueil, which prevents discrimination of the individual effects of run time and fO_2 on the evolution of the spinel Al content, and (2), magnetite-magnesioferrite spinel solid-solution is no longer stable.

Because of the agreement within error between the experimental values and the model, this plot (Fig. 10a) allows, for a given temperature, discrimination of the conjugated effects of run times and fO_2 on the evolution of spinel composition. Conversely, it is possible, knowing the FeO/Fe_2O_3 ratio and the Al_2O_3 content of a spinel, to determine the run time and the oxygen fugacity of the atmosphere ($-0.68 < \log fO_2 < -8$) under which the charge containing the spinel was heated. A similar calculation was performed for a temperature of 1425°C (Fig. 10b). The model also suitably fits the experimental results and shows how increasing the temperature activates the compositional changes of the spinels (Fig. 10a,b).

Finally, if the models obtained for the three temperatures, i.e., 1200, 1350 and 1425°C, are plotted in the same graph (Fig. 11), the sensitivity of the spinel Al_2O_3 content to both the duration and the temperature of the heating-pulse becomes apparent. Thus, this compositional parameter can be a signature of the degree of heating suffered by the charges. However, this correlation is not longer valid for chromium-rich spinels since chromium, aluminum and ferric iron all compete for the same site.

6. APPLICATION TO METEORITIC MATERIALS

With this model in hand, we examine, in the following sections, how cosmic spinel composition may be used (1) to discriminate the different types of extraterrestrial objects entering the Earth's atmosphere and (2) to determine the entry conditions of these objects.

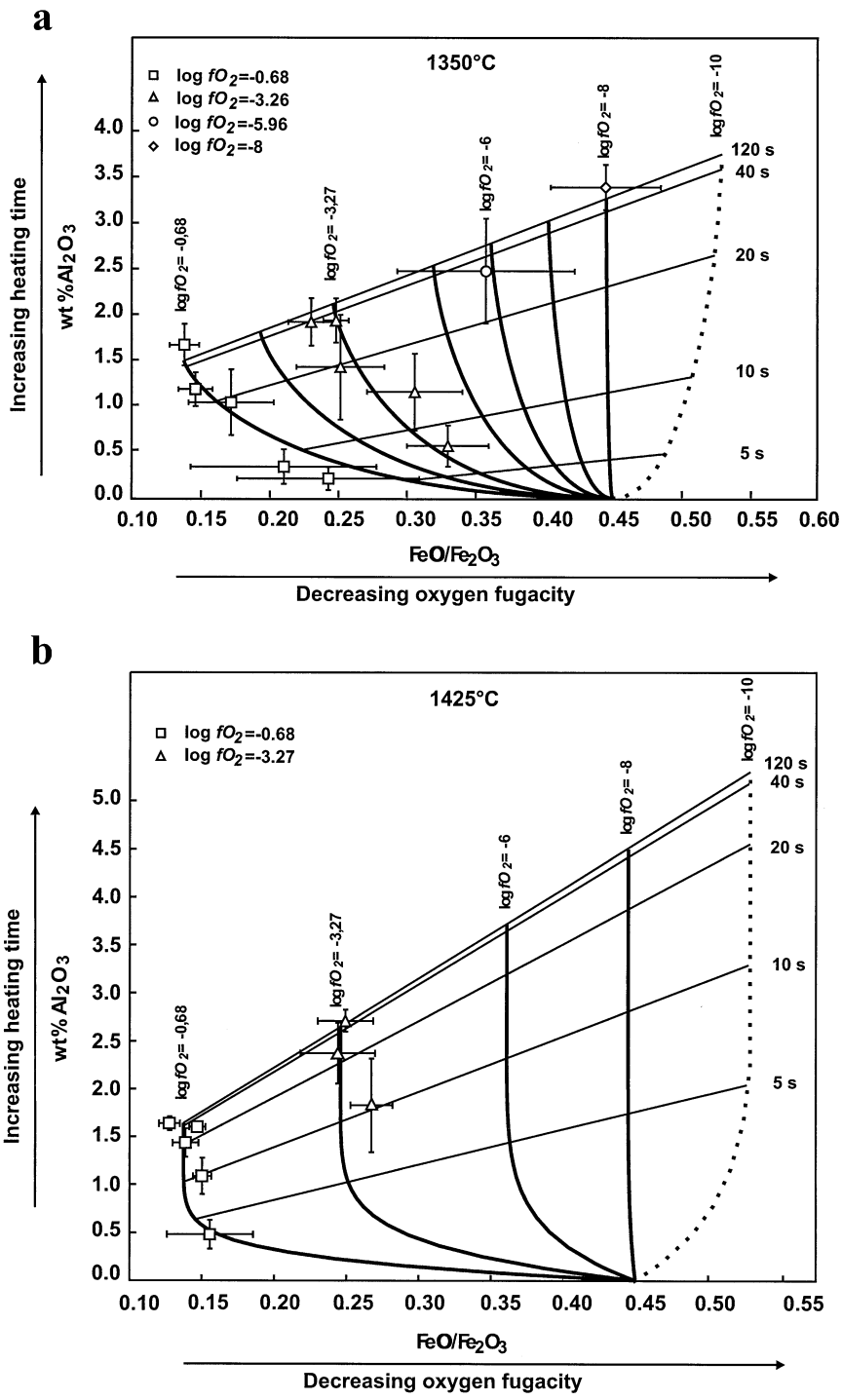

Fig. 10. Al_2O_3 wt% versus FeO/Fe_2O_3 ratio of spinels of pulse-heated charges of Orgueil composition: experimental data (symbols) and spinel composition model (solid lines) (a) at 1350°C and (b) at 1425°C. Bold lines correspond to isofugacity lines and regular lines correspond to isotime lines (see section 4.4.3). Note that the log $fO_2 = -10$ isofugacity line has been extrapolated.

6.1. Factors Controlling Composition of Cosmic Spinels

In the natural environment, our experimental parameter τ (temperature-duration pair) of the heating-pulse stands for the degree of heating or melting (peak temperature and heating duration) suffered by an extraterrestrial object crossing the Earth's orbit. Similarly, experimental oxygen fugacity may be related to the altitude of deceleration of such an object, since

oxygen fugacity is a function of altitude in the Earth's atmosphere. Therefore, we recast our experimental oxygen fugacities in equivalent altitudes using the pressure data at all altitudes of U.S. standard atmosphere 1976 (Weast et al., 1983) and considering a weight fraction of O_2 in air of 1/5 at all altitudes (Fig. 11). The application to extraterrestrial objects is hence straightforward since, according to our modeling (Al_2O_3 vs. FeO/Fe_2O_3 diagram, Fig. 10), the x-axis (FeO/Fe_2O_3 ratio) will indicate the altitude of deceleration of these objects, and the y-axis (Al_2O_3 wt%) the degree of heating they suffered.

Cosmic spinels, belonging to fusion crusts of meteorites (Allende [CV3], Orgueil [CI1], Aumale [L6] and Saint Séverin [LL6]; this study and Robin, personal communication), cosmic spherules and micrometeorites (Table 3) were plotted within the isothermal models of Figure 11. While only representative data are plotted here for simplification, it is apparent that nearly the whole range of cosmic spinels is well reproduced by the models. The sole exceptions are a few cosmic spinels with high-chromium contents and some cosmic spherules containing spinels with very high Al contents (>11 wt% and not shown in the figure) resulting perhaps from partial vaporization (Alexander et al., 2002) or metal loss (e.g., Brownlee and Bates, 1983; Brownlee et al., 1997). This match (see also Fig. 5) demonstrates that our choice of experimental parameters (temperature, time and fO_2) and the choice of Orgueil as a starting material are relevant for understanding the factors that control the composition of cosmic spinels. In the Al_2O_3 vs. FeO/Fe_2O_3 diagram (Fig. 11), spinels from fine-grained MMs with low Al_2O_3 content and FeO/Fe_2O_3 ratios close to 0.45 cluster around $t = 0$; those from scoriaceous MMs delimit a field at higher Al_2O_3 contents and more variable FeO/Fe_2O_3 ratios. Spinels from cosmic spherules and fusion crusts both scatter at high Al_2O_3 contents, but differ in their FeO/Fe_2O_3 ratios, the latter being relatively enriched in ferric iron by comparison with the former. In this diagram, a broad positive correlation is observed for spinels from cosmic spherules and fusion crusts. Thus, in addition to the molten texture of these objects, the high Al_2O_3 content of their spinels and the correlation between their Al_2O_3 content and FeO/Fe_2O_3 ratio are further evidence that cosmic spherules and fusion crusts suffered high degrees of melting. This explains why their spinel compositions mimic the behavior depicted for experimental spinels synthesized in conditions close to equilibrium (~120 s).

According to our experimental results and observations (Engrand and Maurette, 1998; Toppani et al., 2001; this study), differences in spinel composition between these extraterrestrial objects could be mainly related to differences in both degree of heating during atmospheric entry and altitude of deceleration. Increasing Al content of spinels from fine-grained MMs to scoriaceous MMs to cosmic spherules could be mainly related to an increase in the degree of heating. Differences in their FeO/Fe_2O_3 ratios are related both to their degree of heating and to their altitude of deceleration, since our experimental results have shown that the FeO/Fe_2O_3 ratio of spinels, at low τ depends on both extrinsic oxygen fugacity and the degree of heating (temperature and duration of heating). Thus, the determination of the altitude of deceleration of micrometeorites solely with the FeO/Fe_2O_3 ratio of spinels is subject to caution if kinetics factors are not taken into account (Robin et al., 1992). Instead, we strongly advocate the use of the Al_2O_3 vs. FeO/Fe_2O_3 diagram to determine the altitude of deceleration of an extraterrestrial object from its spinel composition. If spinels of meteorite fusion crusts also suggest high degrees of heating, their low Al contents and low FeO/Fe_2O_3 ratios both indicate in contrast that meteorites decelerate at lower altitudes than do cosmic spherules, i.e., in the most oxidizing atmospheric layers (Love and Brownlee, 1991; Robin et al., 1992; Rietmeijer, 2000). For fine-grained and scoriaceous MMs, differences in the FeO/Fe_2O_3 ratio of their spinels with those of fusion crusts may also be attributed to their higher altitudes of deceleration.

Absolute, as well as relative altitudes of deceleration of the different extraterrestrial objects also can be estimated in the light of these results. For small dust particles, it can be assumed that the influence of a gas gasket is negligible and thus, that the oxygen partial pressure around the particle is equivalent to the fO_2 of the atmosphere. With this approximation, we found that altitudes of deceleration of the studied MMs are roughly comprised between 50 and 120 km, while those of cosmic spherules are between 80 and 120 km (Fig. 11), even if a few objects seem to have decelerated higher in the thermosphere. Despite the uncertainties associated with the model, these ranges of deceleration altitudes are consistent with previous models of atmospheric entry of MMs (e.g., Love and Brownlee, 1991) and with observations (Rietmeijer, 2000). For spinels from meteorite fusion crusts, this model shows that they form in the most oxidizing atmospheric layers (between $-0.68 < \log fO_2 < \sim -4$) suggesting deceleration altitudes for meteorites below ~50 km (Robin et al., 1992). However, a more precise determination for meteorites is difficult, since high aerodynamic pressures around the meteorites during their deceleration in the Earth's atmosphere (e.g., Brownlee, 1985; Robin et al., 1992; Hills and Goda, 1993) may significantly affect the oxidation conditions of the surrounding atmosphere and hence the spinel composition ($FeO/Fe_2O_3 < 0.1$ in Fig. 11).

Thus, spinel provides information on the degree of heating and the altitude of deceleration of stony extraterrestrial objects. These parameters are useful for discriminating the different types of stony extraterrestrial objects. Furthermore, since the degree of heating and altitude of deceleration are both related to the mass, the speed and the entry angle of the objects crossing the Earth's orbit, cosmic spinels may also help to constrain the atmospheric entry conditions of extraterrestrial objects.

6.2. Constraints on Entry Angles and Incident Velocities of Extraterrestrial Objects during Their Atmospheric Entry

As cosmic spinels form by rapid crystallization of partial melts produced during meteoroid entry in the Earth's atmosphere, and because the atmosphere surrounding the meteoroid becomes progressively more oxidizing as the meteoroid penetrates deeper in the atmosphere, the spinel compositional range may record the ballistic trajectory of the object during its passage through the Earth's atmosphere. Using case studies from different types of MMs, we also show that these results may be useful for discriminating different objects belonging to a single class of MMs.

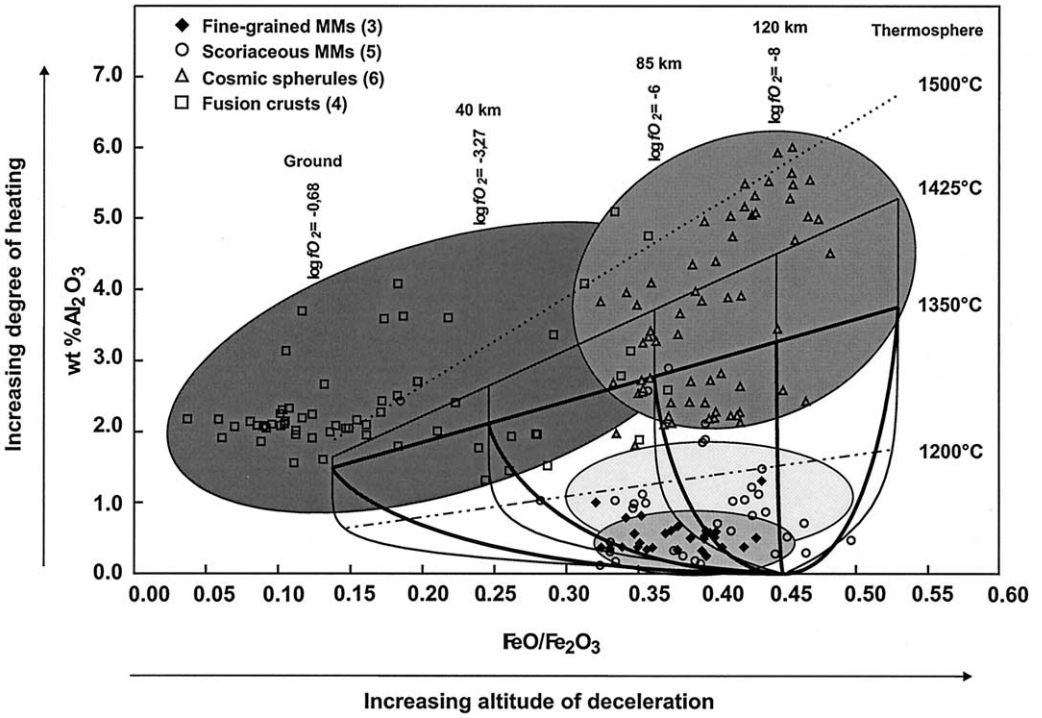

Fig. 11. Classification of the different types of extraterrestrial objects using the Al_2O_3 wt% versus FeO/Fe_2O_3 model obtained at 1200, 1350, 1425 and 1500°C. For clarity, only isofugacity lines are shown together with the 120 s isotime lines. Note that the 120 s isotime line for a temperature of 1500°C has been extrapolated. Cosmic spinels from different extraterrestrial objects, i.e., fine-grained MMs, scoriaceous MMs, cosmic spherules, and fusion crusts (from Allende, Aumale, Orgueil and Saint-Severin chondrites) are reported and gathered inside ellipsoid fields. The correspondence between isofugacity lines and altitudes of deceleration are indicated (see text for interpretation). Numbers in parentheses indicate the number of particles represented for each type of extraterrestrial object.

6.2.1. Fine-Grained and Scoriaceous MMs

We selected here a fine-grained and two scoriaceous large micrometeorites (Table 3) and plotted their spinel compositions in our 1350°C isothermal model (Fig. 12a). Note that all individual spinel compositions probed in each sample, and not average values, were plotted in this graph, and that the choice of the 1350°C isothermal model was made according to the textural characteristics of the samples (low τ, see fig. 11 in Toppani et al., 2001; Toppani and Libourel, 2002).

First, heating durations and altitudes of deceleration were determined for each MM. Figure 12a shows that spinel FeO/Fe_2O_3 ratios of the 3 MMs evolve from 0.45 to lower ratios and Al_2O_3 concentrations increase as the atmosphere and the heating duration become more oxidized and longer, respectively, as the objects fall towards the Earth ′s surface. According to our experimental model, the last spinels to crystallize, those with the highest Al content, provide indications concerning the altitude at which the temperature is low enough to prevent any measurable exchange between the surrounding atmosphere and the melt-spinel system (i.e., the closure temperature of the system by quenching). This is equivalent to the altitude of deceleration at the end of the peak temperature. Accordingly, the fine-grained MM in Figure 12a has been heated for ~ 8 s and ended its deceleration at an altitude of around 50 km. The scoriaceous MMs 1 and 2 have been heated for ~ 20 s and ended their deceleration respectively at 40 and 120 km.

If the scattering of the spinel composition in the Al_2O_3 vs. FeO/Fe_2O_3 diagram is taken into account, entry angles of the 3 MMs in the atmosphere may be compared. Spinels with compositions along an isofugacity line crystallize under roughly constant extrinsic oxygen fugacity. The simplest way to explain this feature is to consider that the MMs entered the Earth's atmosphere at a low entry angle, crystallizing spinels at a fixed altitude under a fairly constant atmosphere. In contrast, spinels trending across several isofugacity lines very likely belong to MMs entering the Earth's atmosphere with higher entry angles and thus crossing several atmospheric layers. The fine-grained MM plotted in Figure 12a must thus have entered the Earth's atmosphere at a higher angle than the two scoriaceous MMs 1 and 2.

Assuming similar sizes and low entry angles for the two scoriaceous MMs, we also suggest that the differences in their altitude of deceleration are very likely due to differences in their incident velocity. MM 2, decelerated high in the atmosphere, most probably entered at a higher speed than did MM 1. This is because a higher speed is required to produce enough heat to partially melt a micrometeorite in the upper atmosphere than in the much denser lower atmosphere.

6.2.2. Cosmic Spherules

Cosmic spherules also show variations in the composition of their spinels (Fig. 11) allowing constraint of their entry condi-

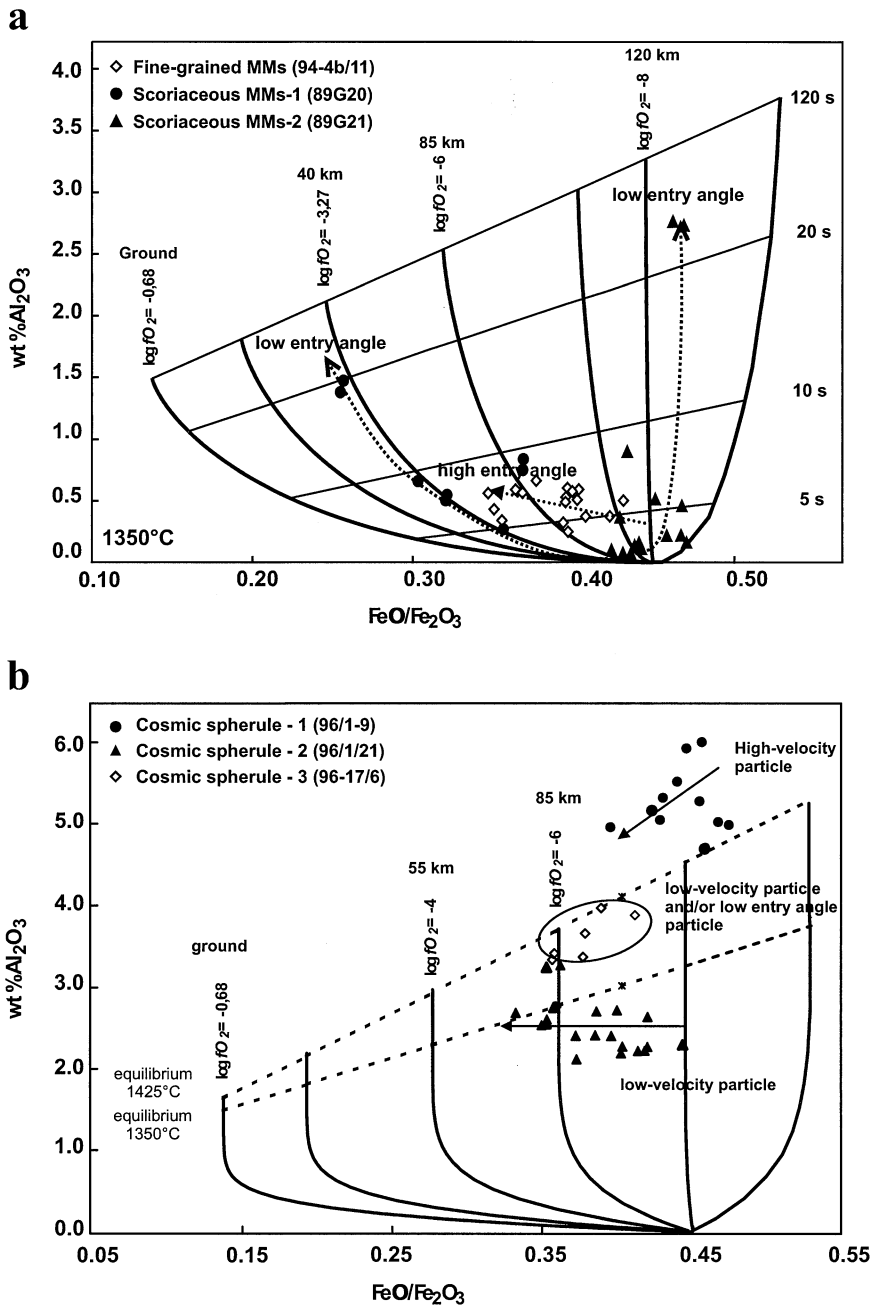

Fig. 12. Determination of the entry conditions of (a) fine-grained and scoriaceous MMs and (b) cosmic spherules using the Al_2O_3 versus FeO/Fe_2O_3 models. In these plots, all spinels probed in a given meteoritic material are reported and their trends are interpreted in term of various entry conditions. In plot (a), spinel composition of the two scoriaceous MMs are from Engrand (1995). Note that in plot (b) cosmic spherule spinels are compared to near equilibrium conditions obtained at 1350°C and 1425°C.

tions in the Earth's atmosphere. The spinels of three large cosmic spherules were plotted in our 1425°C isothermal model (Fig. 12b). We used this high temperature model because of the higher melting rate of these objects. In contrast to less molten objects, Al contents of spinels from individual cosmic spherules are high and decrease with FeO/Fe_2O_3 ratio, either paralleling long duration isotime lines and/or approaching near equilibrium behavior. This means that as spherules penetrate deeper in the Earth's atmosphere, their spinels record more oxidizing conditions, suggesting that the last spinels formed, before the closure of the system, are those with the lowest values of both Al_2O_3 and FeO/Fe_2O_3.

Spherule 1, with spinels with high Al_2O_3 and FeO/Fe_2O_3 contents (Fig. 12b), has been decelerated mainly in the thermosphere, since according to its narrow range of spinel FeO/Fe_2O_3 ratios, only a few atmospheric layers have been crossed. A relatively high incident velocity is suspected for this particle due to its rapid deceleration in a low density atmosphere.

Spherule 2 was decelerated lower in the atmosphere at around 70 km after the crossing of several atmospheric layers, very likely in response to a low entry velocity and a high entry angle. This contrasts with the quite homogeneous spinels found in Spherule 3 suggesting that this spherule decelerated at around 90 km by crossing only few atmospheric layers, due a low velocity and/or a low entry angle conditions.

6.3. Application to the Spinels from the KT Boundary Sediments

Spinels from Cretaceous/Tertiary boundary sediments have long been considered as relics of a major meteoroid impact event (Montanari et al., 1983; Smit and Kyte, 1984; Kyte and Smit, 1986; Robin et al., 1993). However the mechanism of their formation is still a matter of debate. Several authors have proposed that they could either be formed by condensation in the impact plume (e.g., Kyte and Smit, 1986; Ebel and Grossman, 1999) or by ablation of meteoroid material (Kyte and Smit, 1986; Robin et al., 1992).

While spinels from the KT boundary sediments have a morphology similar to those of our synthetic spinels, their compositions can be different depending on their collection sites (Kyte and Bostwick, 1995). KT spinels are indeed characterized by very low FeO/Fe_2O_3 ratios (down to $\sim$ 0), and variable NiO (up to 14 wt%), Al_2O_3 (up to 40 wt%) and MgO (up to 25 wt%) contents. The present study suggests that (i) these spinels have crystallized in a highly oxidant atmosphere, as already suggested by Robin et al. (1992) and (ii) such aluminum and magnesium rich spinels could not have crystallized from a chondritic material as our synthetic spinels (e.g., $Al_2O_3 <$ 10 wt%), but instead from a highly fractionated liquid (Kyte and Bohor, 1995), if they are not products of gas-solid condensation.

7. CONCLUSION

This study shows that pulse-heating experiments on Orgueil starting material performed over a range of temperatures, heating times and oxygen fugacities are able to reproduce the specific morphology and the whole compositional range of cosmic spinels found in fine-grained MMs, scoriaceous MMs, cosmic spherules and fusion crusts of several stony meteorites. Based on these similarities, we infer that cosmic spinels form by crystallization from an iron-rich melt produced by partial melting during the deceleration of the meteoroid in the Earth's atmosphere.

In the light of these experiments, the kinetic evolution of the composition of spinels crystallizing from the Orgueil chondritic material was documented. The cosmic spinel composition, namely the Al_2O_3 content and the FeO/Fe_2O_3 ratio, is found to be dependent on two main parameters: degree of heating (temperature and time) and altitude of deceleration of the meteoroid. Using this variability in the composition of cosmic spinels, it is possible to distinguish unambiguously each class of extraterrestrial objects (i.e., meteorites, fine-grained MMs, scoriaceous MMs and cosmic spherules).

We have shown that, due to the rapid crystallization kinetics of cosmic spinel, the Al_2O_3 content and FeO/Fe_2O_3 ratio of this phase can serve as a tool, if used with caution, to better constrain the entry conditions of meteoritic material in the Earth's atmosphere, i.e., entry angle and incident velocity. Eventually, because extraterrestrial particles entering the Earth's atmosphere can be discriminated based on their velocity (Flynn, 1989), this experimental study and related work (Toppani et al., 2001; Toppani and Libourel, 2002), associated with a numerical model of atmospheric entry of MMs (e.g., Love and Brownlee, 1991), may also provide unique information for distinguishing asteroidal or cometary particles in our collections, before the STARDUST or ROSETTA missions.

Acknowledgments—We are indebted to M. Maurette and C. Engrand for helpful discussions and for their assistance with natural micrometeorites, as well as for providing us with micrometeorites from the French collection (CSNSM, Orsay, France). A. Rouillier is thanked for assistance in the high-temperature experimental laboratory of the CRPG-CNRS. We also thank G. Matrajt and M. Gounelle for help with preparation and handling of the samples and for fruitful discussions. We are also grateful to A. Köhler, R. Podor, F. Diot, S. Barda for assistance with electron microprobe analyses and SEM at the Service d'Analyses of the Université Henri Poincaré, Nancy (France). Meteorite samples were kindly provided by G. Matrajt at CSNSM in Orsay and by F. Robert from the Museum National d'Histoire Naturelle de Paris (MNHN). Fusion crusts of meteorites were also kindly provided by the MNHN. Michelle Bourot-Denise from MNHN is thanked for help in the choice of fusion crusts and for fruitful discussions. We also thank P. Barbey, J. Aléon and L. Reisberg for discussions and comments. The authors are grateful to the Associate Editor C. Koeberl and to G. Kurat and F. T. Kyte for their fast and helpful reviews. This work was supported by INSU through PNP grant (G.L). This is CRPG contribution n° 1637.

Associate editor: C. Koeberl

REFERENCES

Alexander C. M. O.'D., Taylor S., Delaney J. S., Ma P., and Herzog G. F. (2002) Mass-dependent fractionation of Mg, Si and Fe isotopes in five stony cosmic spherules. *Geochim. Cosmochim. Acta* **66,** 173–183.

Barnes S. J. and Roeder P. L. (2001) The range of spinel compositions in terrestrial mafic and ultramafic rocks. *J. Petrol.* **42,** 2279–2302.

Blanchard M. B., Brownlee D. E., Bunch T. E., Hodge P. W., and Kyte F. T. (1980) Meteoroid ablation spheres from deep-sea sediments. *Earth Planet. Sci. Lett.* **46,** 178–190.

Böstrom K. and Fredriksson K. (1966) Surface conditions of the Orgueil meteorite parent body as indicated by mineral associations. *Smithsonian Misc. Coll.* **151,** 1–39.

Brownlee D. E. (1985) Cosmic dust: Collection and research. *Annu. Rev. Earth Planet. Sci.* **13,** 147–173.

Brownlee D. E. and Bates B. (1983) Meteor ablation spherules as chondrule analogs. In *Chondrules and Their Origins* (ed. E. A. King), pp. 10–25. Lunar Planetary Institute.

Brownlee D. E., Bates B., and Schramm L. (1997) The elemental composition of stony cosmic spherules. *Meteorit. Planet. Sci.* **32,** 157–175.

Ebel D. S. and Grossman L. (1999) Condensation in a model chicxulub fireball. *Lunar Planet. Sci.* **30,** 1906.

Engrand C. (1995) Micrometeorites antarctiques: vers l'exoblologie et la mission cométaire "ROSETTA". Ph.D. thesis, Université de Paris Sud, France, 150 pp.

Engrand C. and Maurette M. (1998) Carbonaceous micrometeorites from Antarctica. *Meteori. Planet. Sci.* **33,** 565–580.

Fisk M. R. and Bence A. E. (1980) Experimental crystallization of chrome spinel in famous basalt 527–1–1. *Earth Planet. Sci. Lett.* **48,** 111–123.

Flynn G. J. (1989) Atmospheric entry heating: A criterion to distinguish between asteroidal and cometary sources of interplanetary dust. *Icarus* **77,** 287–310.

Fraundorf P. (1980) The distribution of temperature maxima for micrometeorites decelerated in the Earth's atmosphere without melting. *Geophys. Res. Lett.* **10,** 765–768.

Fruland R. M. (1974) Fusion crust phenomena on some carbonaceous chondrites. *Meteoritics* **9,** 339–342.

Gayraud J., Robin E., Rocchia R., and Froget L. (1996) Formation conditions of oxidized Ni-rich spinel and their relevance to the K/T boundary event. Special Paper 307, pp. 425–443. Geological Society of America.

Genge M. J., Grady M. M., and Hutchison R. (1997) The textures and compositions of fine-grained Antarctic micrometeorites; implications for comparisons with meteorites. *Geochim. Cosmochim. Acta* **61,** 5149–5162.

Genge M. J. and Grady M. M. (1999) The fusion crusts of stony meteorites: Implications for the atmospheric reprocessing of extraterrestrial materials. *Meteor. Planet. Sci.* **34,** 341–356.

Germani M. S., Bradley J. P., and Brownlee D. E. (1990) Automated thin film analyses of hydrated interplanetary dust particles in the analytical microscope. *Earth Planet. Sci. Lett.* **101,** 162–179.

Haggerty S. E. (1976) Opaque mineral oxides in terrestrial igneous rocks. In *Oxide Minerals* (ed. D. Rumble), pp. 101–300. Mineralogical Society of America.

Hallyday I., Blackwell A. T., and Griffin A. A. (1989) The typical meteorite event, based on photographic records of 44 fireballs. *Meteoritics* **24,** 65–72.

Hill R. and Roeder P. (1974) The crystallization of spinel from basaltic liquid as a function of oxygen fugacity. *J. Geol.* **82,** 709–729.

Hills J. G. and Goda M. P. (1993) The fragmentation of small asteroids in the atmosphere. *Astron. J.* **105,** 1114–1144.

Hyman M., Rowe M. W., and Herndon J. M. (1978) Magnetite heterogeneity among CI chondrites. *Geochem. J.* **13,** 37–39.

Hyman M. and Rowe M. W. (1983) Magnetites in CI chondrites. *Lunar Planet. Sci.* **13,** A736–A740.

Jessberger E. K., Bohsung J., Chakaveh S., and Traxel K. (1992) The volatile element enrichment of chondritic interplanetary dust particles. *Earth Planet. Sci. Lett.* **112,** 91–99.

Keller L. P., Thomas K. L., and McKay D. S. (1992) Thermal processing of cosmic dust: Atmospheric heating and parent body metamorphism. *Lunar Planet. Sci.* **23,** 675–676.

Keller L. P., Thomas K. L., and McKay D. S. (1993) Carbon abundances, major element chemistry, and mineralogy of hydrated interplanetary dust particles. *Lunar Planet. Sci.* **24,** 785–786.

Keller L. P., Thomas K. L., and McKay D. S. (1996) Mineralogical changes in IDPs resulting from atmospheric entry heating. In *Physics, Chemistry, and Dynamics of Interplanetary Dust—Proceedings of the 150th Colloquium of the International Astronomical Union* (eds. B. A. S. Gustafson and M. S. Hanner), pp. 295–298. Astronomical Society of the Pacific Conferences Series, Gainesville.

Kerridge J. F. (1970) Some observations on the nature of magnetite in the Orgueil meteorite. *Earth Planet. Sci. Lett.* **9,** 299–306.

Kerridge J. F., MacDougall J. D., and Marti K. (1979) Clues to the origin of sulfide minerals in CI chondrites. *Earth Planet. Sci. Lett.* **43,** 359–367.

Kyte F. T. and Smit J. (1986) Regional variations in spinel compositions: An important key to the Cretaceous/Tertiary event. *Geology* **14,** 485–487.

Kyte F. T. and Bohor B. F. (1995) Nickel-rich magnesiowüstite in Cretaceous/Tertiary boundary spherules crystallized from ultramafic, refractory silicate liquids. *Geochim. Cosmochim. Acta* **59,** 4967–4974.

Kyte F. T. and Bostwick J. A. (1995) Magnesioferrite spinel in Cretaceous/Tertiary boundary sediments of the Pacific basin: Remnants of hot, early ejecta from the Chicxulub impact? *Earth Planet. Sci. Lett.* **132,** 113–127.

Kurat G., Koeberl C., Presper T., Brandstätter F., and Maurette M. (1994) Petrology and geochemistry of Antarctic micrometeorites. *Geochim. Cosmochim. Acta* **58,** 3879–3904.

Love S. G. and Brownlee D. E. (1991) Heating and thermal transformation of micrometeoroids entering the Earth's atmosphere. *Icarus* **89,** 26–43.

Maurel C. and Maurel P. (1982a) Etude expérimentale de la distribution de l'aluminium entre bain silicaté basique et spinelle chromifère. Implications pétrogénétiques: Teneur en chrome des spinelles. *Bull. Mineral.* **105,** 197–202.

Maurel C. and Maurel P. (1982b) Etude expérimentale de la solubilité du chrome dans les bains silicatés basiques et de sa distribution entre liquide et minéraux coexistants: Conditions d'existence du spinelle chromifère. *Bull. Mineral.* **105,** 640–647.

Maurel C. and Maurel P. (1983) Influence du fer ferrique sur la distribution de l'aluminium entre bain silicaté basique et spinelle chromifère. *Bull. Mineral.* **106,** 623–624.

Maurel C. and Maurel P. (1984) Etude expérimentale de la distribution du fer ferrique entre spinelle chromifère et bain silicaté basique. *Bull. Mineral.* **107,** 25–33.

Maurette M. (1998) Carbonaceous micrometeorites and the origin of life. *Orig. Life Evol. Biosphere* **28,** 385–412.

Maurette M., Olinger C., Christophe Michel-Levy M., Kurat G., Pourcher M., Brandstätter F., and Bourot-Denise M. (1991) A collection of diverse micrometeorites recovered from 100 tonnes of Antarctic blue ice. *Nature* **351,** 44–47.

Montanari A., Hay R. L., Alvarez W., Asaro F., Michel H. V., Alvarez L. W., and Smit J. (1983) Spheroids at the Cretaceous-Tertiary boundary are altered impact droplets of basaltic composition. *Geology* **11,** 668–671.

Nagy B. and Claus G. (1962) Notes on the petrography of the Orgueil meteorite. In Advances in Organic Chemistry. *Proc. Intern. Meeting Milan* (eds. U. Colombo and G. D. Hobson), pp. 115–118. Pergamon.

Ramdohr P. (1967) Die Schmelzkruste der Meteoriten. *Earth Planet. Sci. Lett.* **2,** 197–209.

Rietmeijer F. J. M. (2000) Interrelationships among meteoric metals, meteors, interplanetary dust, micrometeorites, and meteorites. *Meteor. Planet. Sci.* **35,** 1025–1041.

Rietmeijer F. J. M. and Nuth J. A. III. (2000) Collected extraterrestrial materials: Constraints on meteor and fireball compositions. *Earth Moon Planets* **82–83**, 325–350.

Robin E., Bonté Ph., Froget L., Jéhanno C., and Rocchia R. (1992) Formation of spinels in cosmic objects during atmospheric entry: A clue to the Cretaceous-Tertiary boundary event. *Earth Planet. Sci. Lett.* **108,** 181–190.

Robin E., Froget L., Jéhanno C., and Rocchia R. (1993) Evidence for a K/T impact event in the Pacific Ocean. *Nature* **363,** 615–617.

Schreiber H. D. and Haskin L. A. (1976) Chromium in basalts: Experimental determination of redox states and partitioning among synthetic silicate phases. *Proc. Lunar Sci. Conf.* **7,** 513–538.

Smit J. and Kyte F. T. (1984) Siderophile-rich magnetic spheroids from the Cretaceous-Tertiary boundary in Umbria, Italy. *Nature* **310,** 403–405.

Tomeoka K. and Buseck P. R. (1988) Matrix mineralogy of the Orgueil CI carbonaceous chondrite. *Geochim. Cosmochim. Acta* **52,** 1627–1640.

Toppani A., Libourel G., Engrand C., and Maurette M. (2001) Experimental simulation of atmospheric entry of micrometeorites. *Meteor. Planet. Sci.* **36,** 1377–1396.

Toppani A. and Libourel G. (2002) Experimental study of micrometeorite vesiculation. *Lunar Planet. Sci.* **33,** 1473.

Weast R. C., Astle M. J., and Beyer W. H. (1983) *Handbook of Chemistry and Physics* (ed. R. C. Weast), pp. F155–F157. CRC Press.

Whipple F. L. (1951) The theory of micrometeorites, 2. In a heterothermal atmosphere. *Proc. Nat. Acad. Sci. USA* **37,** 19–30.